How Far Does a Rocket Turn Into the Wind?

Rev 1.1

Sept 21, 2024

Thomas B Fetter

Summary

When a rocket leaves the launch guide, it is subject to a step in the lateral wind velocity that causes the rocket to turn or rotate into the direction of the oncoming wind. Conventional wisdom has it that the greater the distance between the center of pressure and center of gravity, also known as the stability margin, the more a rocket will rotate into the wind due to the longer moment arm between the center of pressure and center of gravity. Using a 2-dimensional nonlinear flight model and a series sensitivity analysis, it is shown what impact various rocket design parameters have on how far the rocket rotates. It is also shown that there is not a direct correlation between the stability margin and how far the rocket rotates. That is, being "over stable" is not necessarily an indication a rocket will be more susceptible to rotating into the wind. It is shown having a higher thrust to weight ratio has the biggest impact on minimizing the rotation into the wind.

Table of Contents

1 Introduction

1.1 Objective and Approach

As a rocket leaves the launch guide, it is subject to step in the velocity of the wind, creating a normal force that causes the rocket to rotate into the direction of the oncoming wind. This paper looks at the magnitude of the angle of rotation in response to the step in wind velocity. Because the initial step in wind velocity is large relative to the velocity of the rocket as it leaves the launch guide, and because the resulting rotation of the rocket takes place during a large change in the velocity of the rocket as it accelerates under the thrust of the motor, a linearized rotational model[1] is not valid, so the complete nonlinear flight model[2] must be used to analyze the rocket's rotation. Small perturbations in wind velocity can impact the rotation of the rocket throughout its flight but it is the large step in relative velocity as the rocket leaves the launch guide that drives the flight trajectory of the rocket.

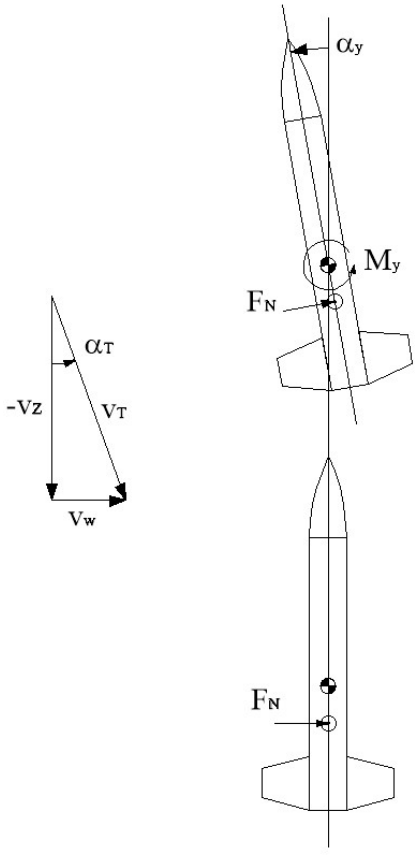

Figure 1-1 Rotation into the wind

[1] (Fetter T. B., 2024, pp. 25-33)

[2] See Appendix 3 – 2-D Flight Model

The term "over stable" is often used to describe a rocket with the stability margin much greater than one[3]. The stability margin in this case is measured by the distance between the center pressure and the center of gravity of the rocket. It is believed that a rocket that is over stable would be more prone to rotating further in response to a wind perturbation because of a larger moment arm between the center of pressure and center of gravity. And with an increase in the flight path angle, the expected maximum altitude would decrease. This paper includes a look at the relationship between the stability margin and the magnitude of the rocket's rotation into the wind and the impact on the maximum altitude of the rocket.

1.2 Prior Work

The rotational dynamics and flight trajectory model used for this analysis is based primarily on the material in the book *Topics in Advanced Model Rocketry*[4], in particular the chapter *A Unified Approach to Aerodynamic Stability*, by Gordon K. Mandell, and the chapter *Elements of Trajectory Analysis* by George J. Caporaso.

Mandell uses Barrowman's static stability equations[5] to determine the rotational forces on the rocket. Barrowman's work is based on NACA research on determining the stability of aerodynamically stabilized sounding rockets. Barrowman simplified the methods for the set of flight conditions that apply to model rockets. He developed a unified method for predicting the static stability of model rockets by calculating the aerodynamic center of pressure. This work was presented at NARAM 8[6] and published in *TIR-33 Calculating the Center of Pressure of a Model Rocket*[7], and *TIR-30 Stability of a Model Rocket in Flight*[8]. Barrowman also derived the rotational damping moment term that is used in the rotational dynamics equation[9].

Some of the tools and models used in this paper are based on prior work done by the author to model and visualize a rocket's flight in 3-dimensional space. Those same tools were also used to visualize the measured flight data from

---

[3] TIR-30 (Barrowman J. , 1970, p. 12)

[4] (Mandell, Caporaso, & Bengen, 1973).

[5] (Barrowman J. S., The Practical Calculation of the Aerodynamic Characteristics of Slender Finned Vehicles, Master's Thesis, 1967)

[6] (Barrowman & Barrowman, The Theoretical Prediction of Center of Pressure, NARAM-8, 1966)

[7] (Barrowman J. , 1968)

[8] (Barrowman J. , 1970)

[9] (Barrowman J. S., The Practical Calculation of the Aerodynamic Characteristics of Slender Finned Vehicles, Master's Thesis, 1967, p. 40)

an RAF Datalogger board. The modeling is done in Mathcad[10], and the flight and attitude visualization is written using the Visual Python library in Python. Examples of this work are available on the authors web site[11], but it otherwise it has not been published to date.

[10] (Mathcad Home Page, n.d.)

[11] (Fetter T. , 2014-2016)

2 Modeling the Wind Rotation

2.1 Rotation Angles

There are five rotational angles of interest. Figure 2-1 and Figure 2-2 show the definitions of these five angles[12].

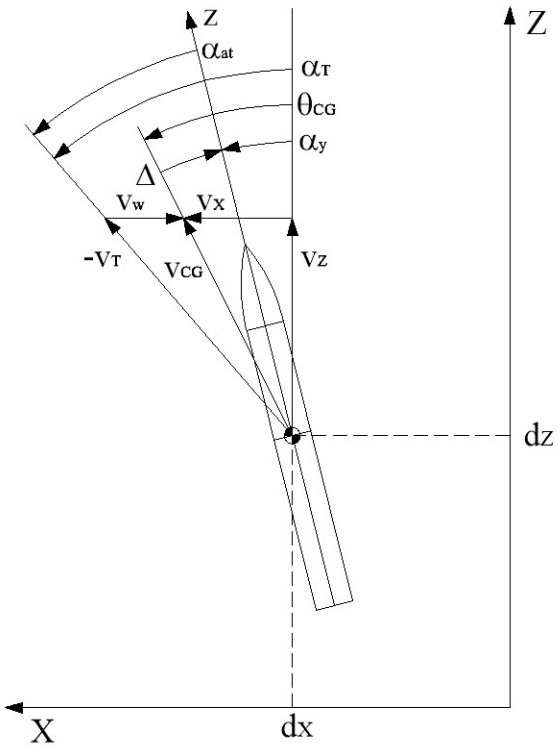

Figure 2-1 Key rotational angles

[12] See Appendix 3 – 2-D Flight Model for a description of the frame of reference axis conventions used in this paper

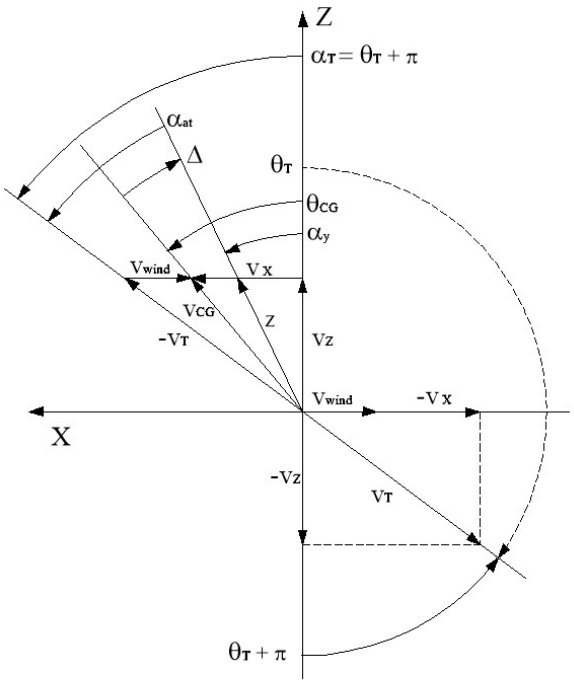

Figure 2-2 Key velocity vectors and angles

The angle of the rocket's rotation, α_y, as shown in Figure 2-1 describes the rocket's rotational response to the wind. The α_y notation is used because the rocket is rotating about the implied y-axis which is coming out of the plane of the of the figure in a right hand coordinate system. The angle is measured from the vertical Z-axis, with positive angles measuring the counterclockwise distance from the vertical Z-axis. The first quadrant is the upper left quadrant of the graph.

α_T is the angle of the oncoming airstream in the first quadrant, and is the input angle to the rotational equation that drives the rocket's rotation. α_T is determined by the sum of the negative of X-axis velocity of the rocket plus the lateral wind velocity and the negative of the Z-axis velocity of the rocket as shown in Figure 2-2.

θ_{CG} is the angle of the motion of the center of gravity of the rocket, which is determined by the X and Z-axis velocities of the rocket.

α_{at} is the angle of attack which is the angle of inclination of the rocket's z-axis to the direction of the total oncoming airstream.

The center of gravity of the rocket can be moving in a direction that is not the same as the direction in which it is pointed if there is a lateral wind. Δ is the angle between the angle of the flight path and the angle in which the rocket is pointed.

2.2 Rotation Due to Wind at Launch

The complete 2-D flight that is derived in Appendix 3 – 2-D Flight Model, along with the definitions of the forces and coefficients, solves for the state variables of the system, $d_X, v_X, d_Z, v_Z, \alpha_y,$ and ω_y, which completely describe the state of the system at any point in time. The inputs to the model are the wind velocity, v_w, and the thrust of the motor. Each of the other rotational angles can then be solved as algebraic functions of the state variables.

$$m_o \frac{d^2 d_X}{dt^2} = F_{TX} + F_{DX} + F_{LX}$$

$$m_o \frac{d^2 d_Z}{dt^2} = F_{TZ} + F_{DZ} + F_{LZ} - m_o g$$

$$I_L \cdot \frac{d^2}{dt^2}\alpha_y + C_2 \cdot \frac{d}{dt}\alpha_y + C_1 \cdot \alpha_y = C_1 \cdot \alpha_T$$

Figure 2-3 shows the rotation angle of the rocket, α_y, and the angle of the total oncoming airstream, α_T, from the complete flight model for test rocket TR-1, shown in Section 3.1, with a 10 mph step in wind velocity occurring as the rocket leaves the launch guide at 0.0264 seconds and with motor burnout at 1.3 seconds. α_T is the input to the rotational equation, and α_y is the output. The initial step in input angle seen by the rocket as it leaves the launch guide is 11.1 degrees. The rocket then starts its rotation to align itself with the direction of the oncoming total airstream. α_T then changes over time due its coupling with the X and Z-axis equations of motion through the lift force[13] and the rocket velocity.

[13] See (Fetter T. B., 2024) , Section 2.2, for a complete description of the coupling mechanisms between the equation in the flight model

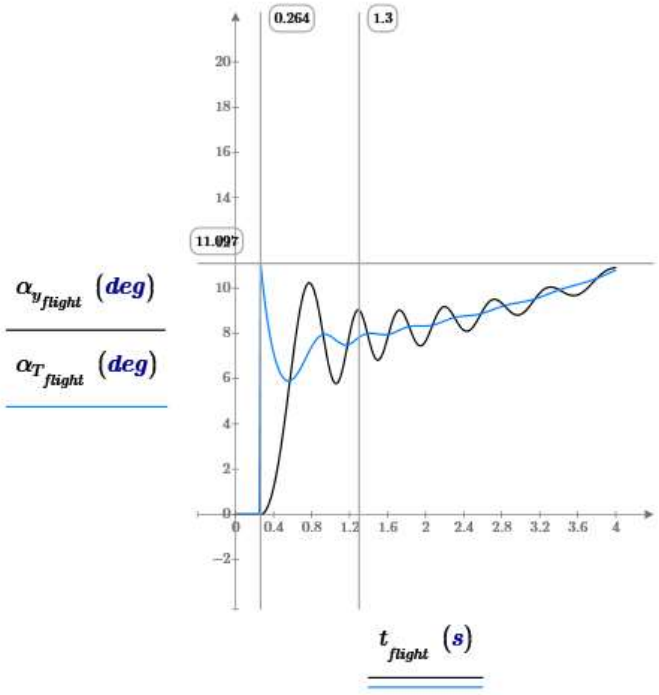

Figure 2-3 Angle of the total oncoming airstream, α_T and the rocket rotation angle, α_y

From Figure 2-1, for small angles of rotation,

$$\alpha_T = \arcsin\left(\frac{v_X - v_w}{v_T}\right) \simeq \frac{v_X}{v_T} - \frac{v_w}{v_T} \tag{2.2-1}$$

so the total oncoming airstream angle is comprised of two terms, one proportional to the wind velocity, and the other proportional to the X-axis velocity. Figure 2-4 shows each of these terms. The term due to the wind velocity starts out at ∞ because the velocity of the oncoming airstream starts out at 0 when the rocket is first launched, but the rocket does not actually see the wind term until is leaves the launch guide at 0.264 seconds into the flight, where the rocket, in this case, is traveling at 51 mph. The combination of the 10 mph wind velocity and the 51 mph forward velocity creates an initial oncoming airstream angle of 11.097 deg as seen in Figure 2-4. The wind term continues to decrease as the total airstream velocity increases with the rocket's acceleration until motor burnout at 1.3 seconds, as shown in Figure 2-6. The airstream velocity then decreases due to the rocket's deceleration due to gravity, and the wind component to the airstream angle slowly increases.

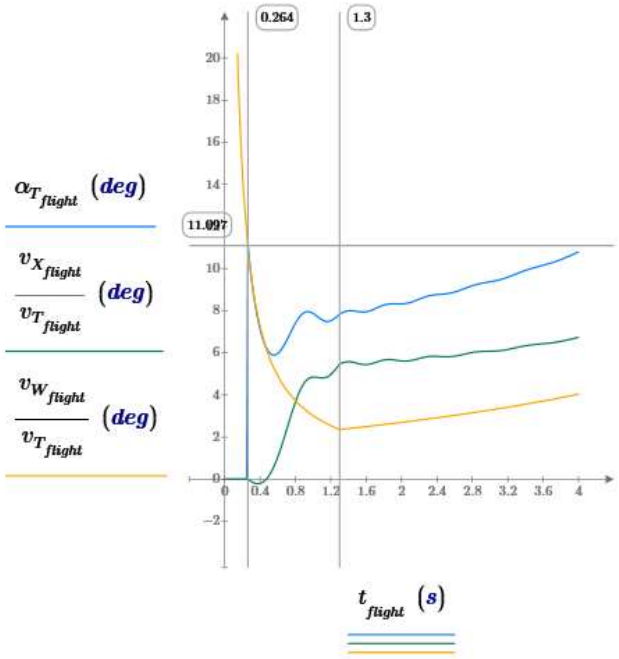

Figure 2-4 Terms that comprise the angle of the oncoming airstream

The second component of the angle of the oncoming airstream, α_T , is due to the X-axis velocity of the rocket. After the rocket starts its rotation, as shown in Figure 2-5 , there is a component of the thrust aligned with the X-axis, and the rocket starts to accelerate along the X-axis, as shown in shows Figure 2-6. Figure 2-5 shows that the ratio of the X-axis velocity to the total airstream velocity increases as a step function until it reaches a nearly fixed ratio between the two velocities as the rocket completes its initial turn. The X-axis velocity then tracks the total airstream velocity from that point forward. The time it takes the ratio to reach a fixed value depends on both the time it takes the rocket to rotate and the time it takes for the initial acceleration along the X-axis.

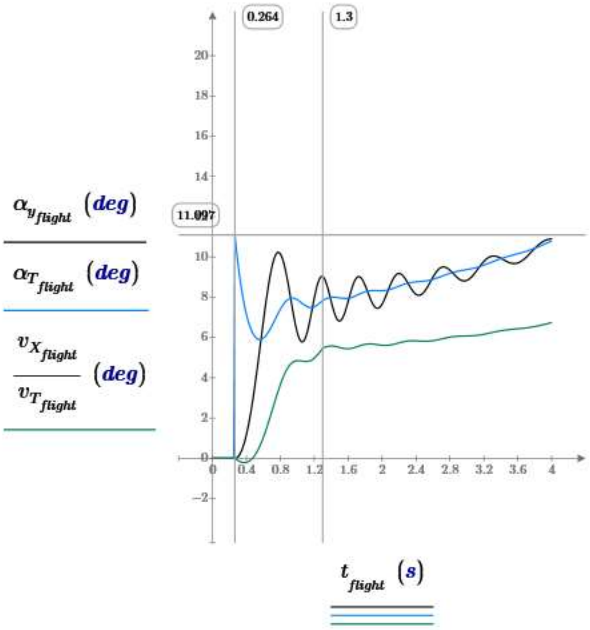

Figure 2-5 X-axis velocity increases after rocket rotates

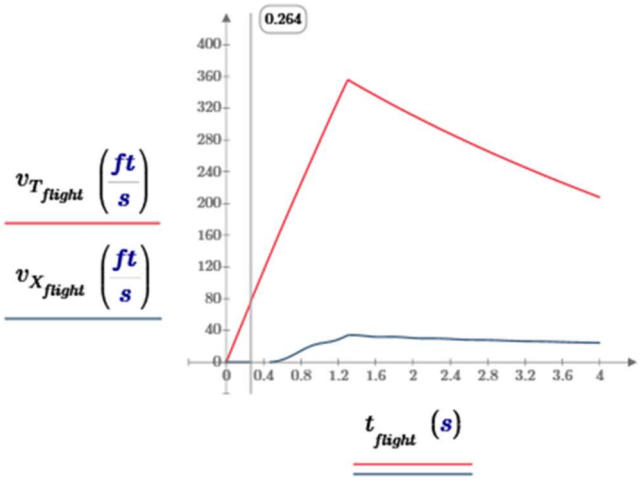

Figure 2-6 Total airstream velocity and rocket X-axis velocity

It is hard to see the actual angle of rotation of the rocket from the ground during its flight because the rocket is a long distance from the observer and is moving very rapidly. The angle of the flight path is more likely what an observer on the ground will see as an indication of how far the rocket has turned into the wind as it is clearly delineated by the exhaust trail of the motor. As the rocket rotates into the wind, there is a component of the thrust that is aligned with the X-axis, and the rocket starts to accelerate along the X-axis, resulting in a change in the angle

of the flight path. The flight path angle, θ_{CG} , is the angle of a line tangent to the motion of the center of gravity of the rocket and is a measure of the deviation from a vertical flight path at any point along the flight path. Figure 2-7 shows that the flight path angle is the ratio of the X-axis velocity to the Z-axis velocity for small flight path angles.

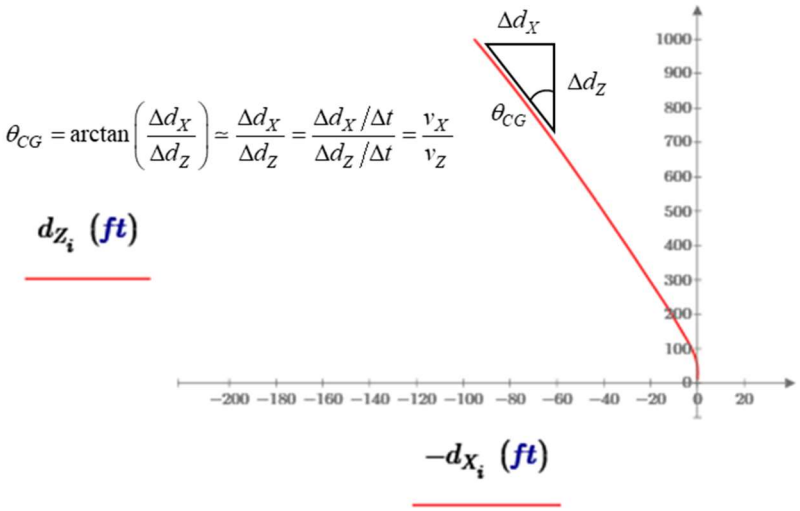

Figure 2-7 Angle of the flight path tangent θ_{CG}

Figure 2-8 shows that the total airstream velocity is very close to the Z-axis velocity of the rocket since $v_Z >> (v_w - v_X)$. Therefore

$$v_T = \sqrt{(v_X - v_w)^2 + v_Z{}^2} \simeq v_Z$$

and

$$\theta_{CG} \simeq \frac{v_X}{v_T} \tag{2.2-2}$$

which is the X-axis velocity component of the angle of the total oncoming airstream in equation (2.2-1). Therefore, the angle of the oncoming airstream equals the flight path angle plus the ratio of the wind to total velocity

$$\alpha_T \simeq \theta_{CG} - \frac{v_w}{v_T} \tag{2.2-3}$$

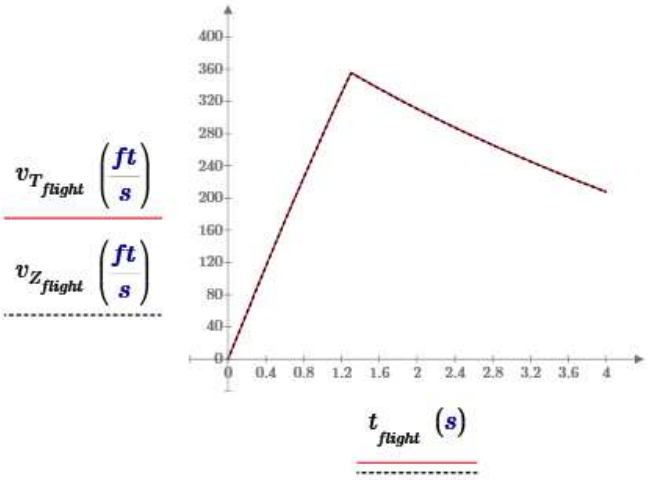

Figure 2-8 Z-axis velocity and total airstream velocity

Figure 2-9 shows all the key rotational angles where v_X / v_T is the flight path angle

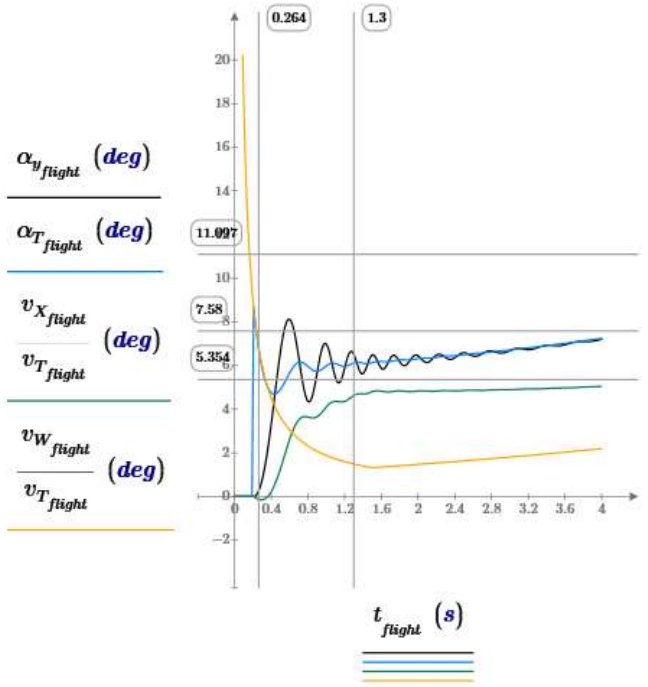

Figure 2-9 Key rotational angles where the green trace, $\frac{v_X}{v_T} \simeq \theta_{CG}$, the flight path angle

The angle of attack is the difference between the angle of the total oncoming airstream and the angle of the rotation of the rocket. The angle of the oncoming airstream is the input that drives the rotational equation, and the rotational step response eventually settles to the input angle, α_T, where the angle of attack, α_{at}, goes to zero. The normal force, which causes the rocket to rotate, is proportional to the angle of attack. At equilibrium, the angle of attack and the normal force go to 0, and the rocket stops rotating.

$$\alpha_{at} = \alpha_T - \alpha_y \tag{2.2-4}$$

$$\alpha_y\Big|_{t\to\infty} = \alpha_T$$

$$\alpha_{at}\Big|_{t\to\infty} = 0$$

Figure 2-10 shows that the angle of attack starts at 11.097 deg as the rocket leaves the launch guide and settles to 0 deg as the rocket reaches equilibrium.

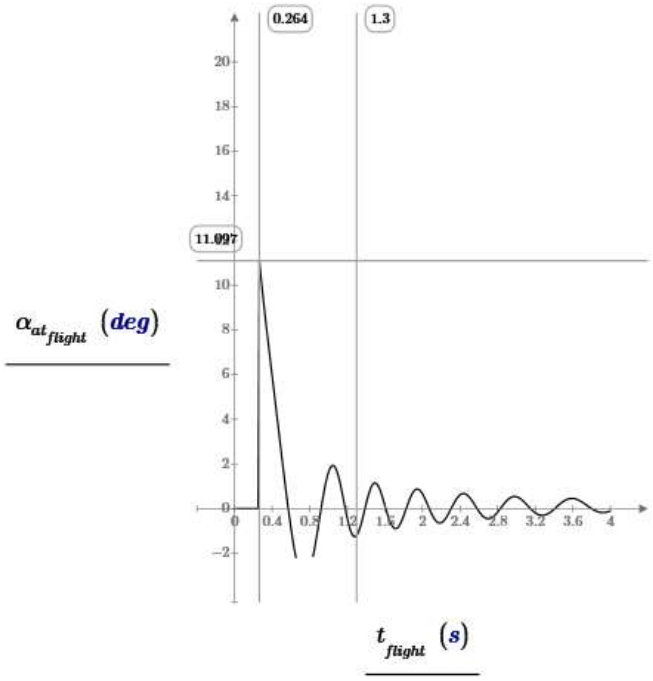

Figure 2-10 Angle of attack

Figure 2-11 shows the angle between the angle of the rocket's rotation and the angle of the flight path, Δ. The rocket does not necessarily fly in the direction that it is pointed.

$$\Delta = \alpha_y - \theta_{CG} \tag{2.2-5}$$

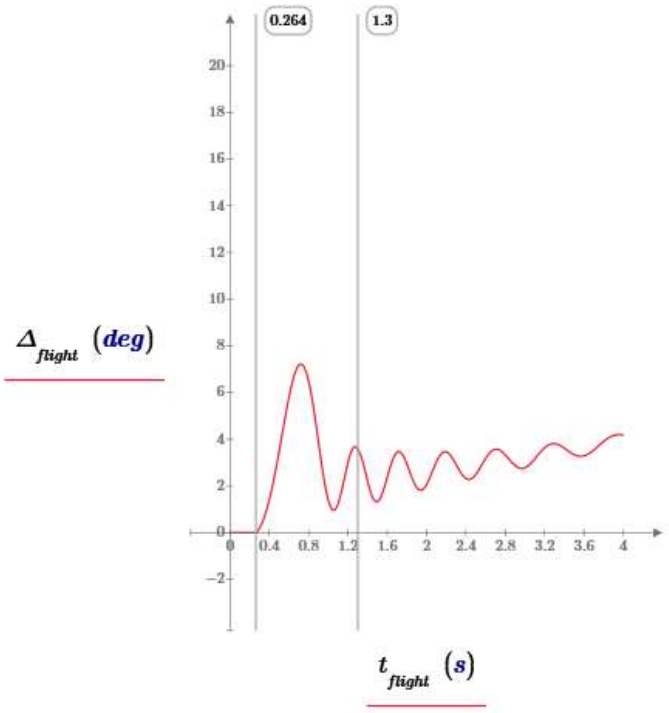

Figure 2-11 The difference angle between the angle of the rocket's rotation and the angle of the flight path

Solving for Δ as $t \to \infty$ and the angle of attack goes to 0,

$$\Delta = \alpha_y - \theta_{CG} = \alpha_y - \frac{v_X}{v_T}$$

$$\alpha_y\Big|_{t\to\infty} = \alpha_T = \frac{v_X}{v_T} + \frac{v_w}{v_T}$$

$$\Delta\Big|_{t\to\infty} = \frac{v_w}{v_T} \simeq \frac{v_w}{v_Z} \tag{2.2-6}$$

so the angle between the direction the rocket is pointed and the angle of the flight path converges on the ratio of the velocity of the wind and the velocity of the rocket, as shown in Figure 2-12

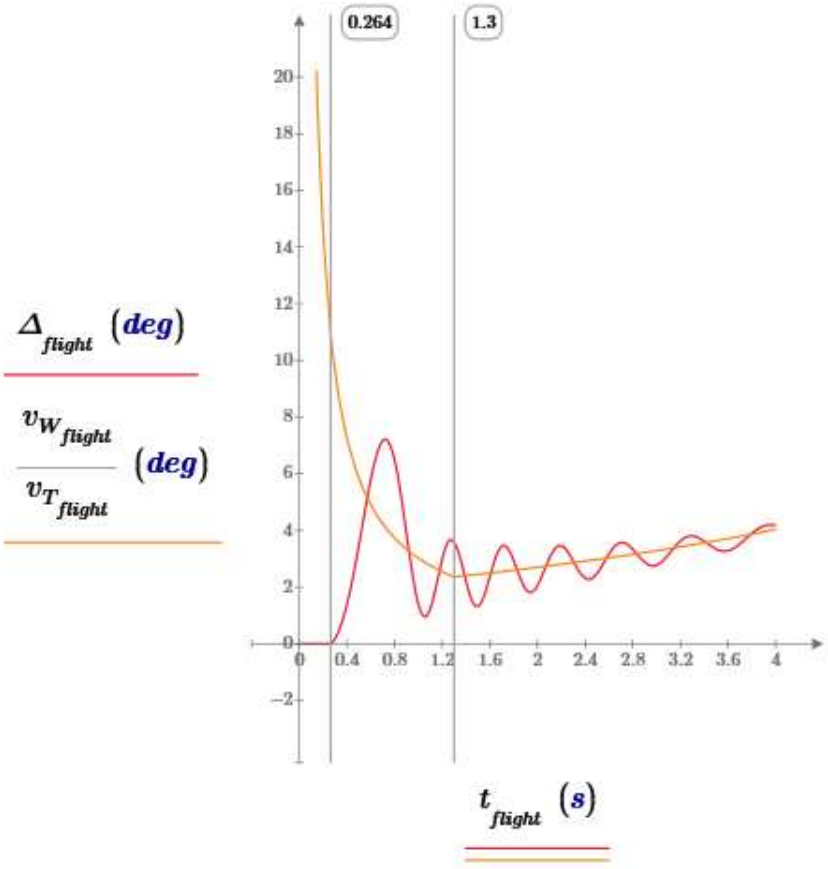

Figure 2-12 Showing Δ converges on $v_w/v_T \simeq v_w/v_Z$

Figure 2-13 shows the angles from Figure 2-1 when $\alpha_y = \alpha_T$ and $\alpha_{at} = 0$, once the rocket rotation has reached its equilibrium value. Once the angle of attack has gone to zero, there is no longer a normal force that would cause further rotation of the rocket. The direction of the oncoming airstream, v_T, is just the sum of the rockets velocity vector plus the oncoming wind. The difference between the center of gravity vector, v_{CG}, and the oncoming airstream vector, with which the rocket is aligned, is the wind vector, v_w, and the angle is $v_w/v_T \simeq v_w/v_Z$. So, the rocket flies at an angle which is the ratio of the wind velocity to the forward velocity of the rocket.

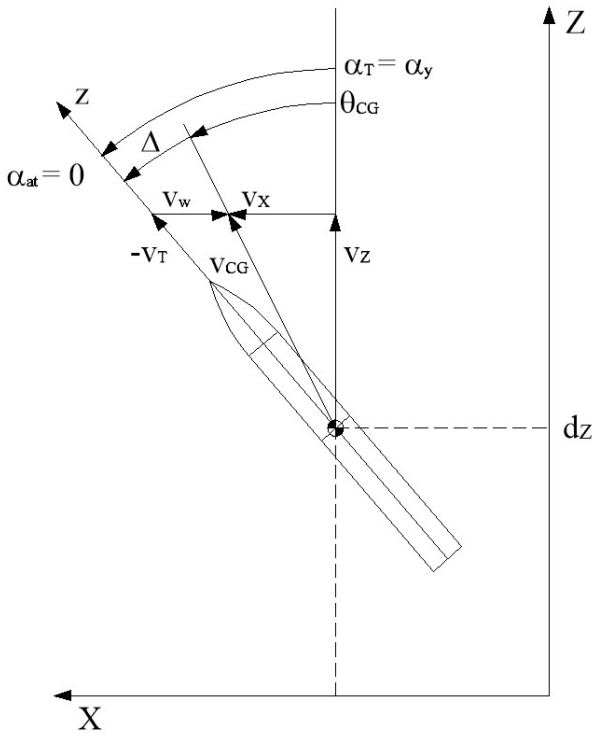

Figure 2-13 Rocket orientation and angles at equilibrium when $\alpha_{at} = 0$

2.3 The Gravity Turn

Figure 2-14 shows the rocket rotation and flight path angles for test rocket TR-1 flying on an H128W in a 10 mph wind. In response to the step in wind velocity as the rocket leaves the launch guide, the rocket rotates 7.58 deg at motor burnout at 1.3 sec. The flight path angle is about 2 degrees less at 5.35 deg at motor burnout. But after motor burnout, both the rocket rotation angle and the flight path angle continue to increase slowly. That slow increase in rotation is due to gravity.

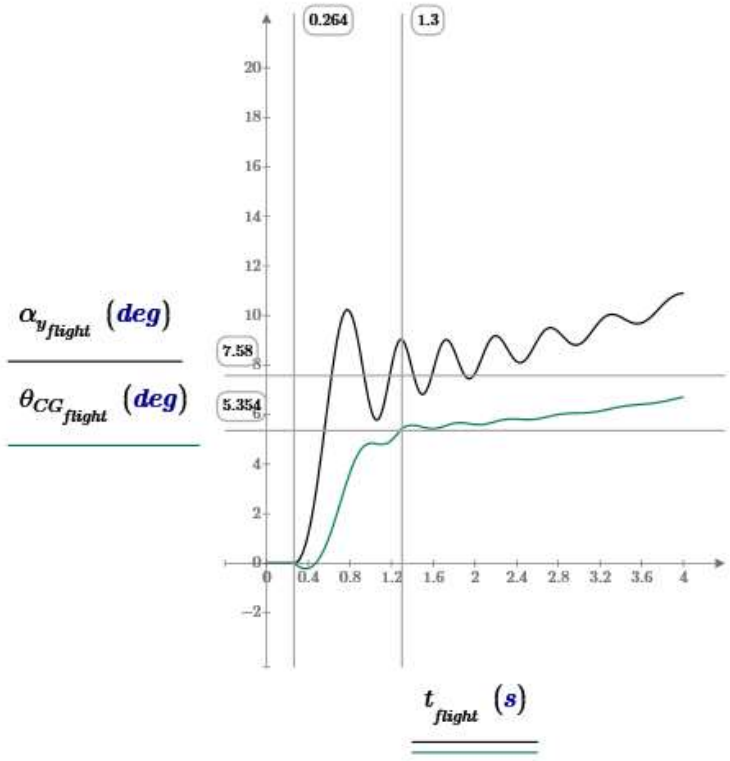

Figure 2-14 Rocket rotation and flight path angles

Once the rocket's flight path angle has turned away from vertical, the flight path will continue to turn because of the acceleration due to gravity. Figure 2-15 shows the trajectory for an object with an initial velocity of $v_{X(0)}$ and $v_{Z(0)}$ for a series of discrete time segments. In each time segment, the initial horizontal velocity, $v_{X(n-1)}$, remains constant if the effect of drag is not included, but the vertical velocity at the start of the each segment, $v_{Z(n-1)}$ is decreased by $g \cdot \Delta t$ from the starting velocity of the previous segment. As a result, the angle of the flight path trajectory, θ_{CG}, increases with each segment, and trajectory arcs over.

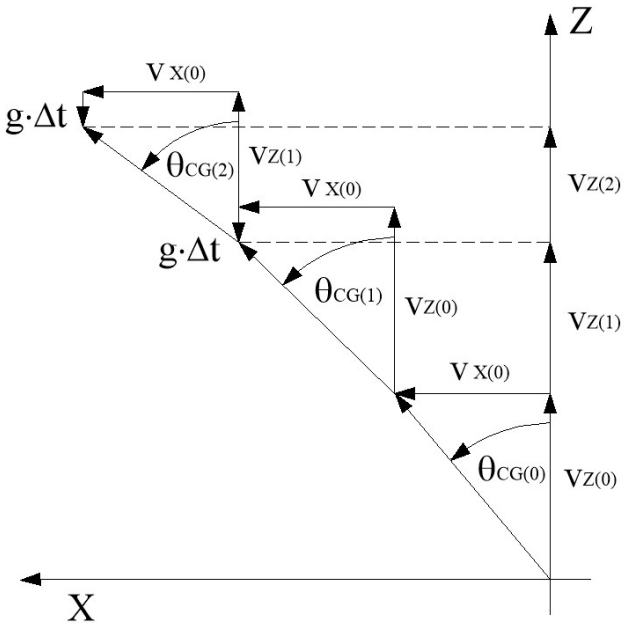

Figure 2-15 The gravity turn where $v_{Z(n+1)} = v_{Z(n)} - g \cdot \Delta t$

In continuous time, the Z-axis velocity can be calculated by

$$a = \frac{dv}{dt} = \frac{d^2x}{dt^2}$$

$$d_x = \int v_X \cdot dt = v_X \cdot t$$

$$d_x = \int v_X \cdot dt = v_X \cdot t$$

$$d_Z = -\int\int g \cdot dt = -\frac{1}{2} \cdot g \cdot t^2 + v_{Z(0)} \cdot t + d_{Z(0)} \tag{2.3-1}$$

Plotting the Z-axis position, d_Z, versus the X-axis position, d_X, produces a parabolic curve due to the t^2 term in d_Z.

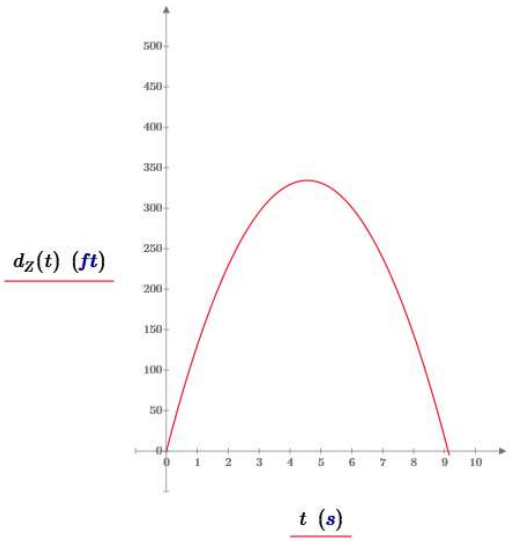

Figure 2-16 Plot of (2.3-1) for $v_{Z(0)} = 100 \cdot mph$ and $v_X - 10 \cdot mph$

Figure 2-17 shows the flight trajectory for test rocket TR-1 showing the initial turn due to the step in wind as the rocket leaves the launch guide, and the longer term gravity turn. Once the rocket flight path angle has rotated 90 degrees, the rocket is no longer gaining altitude, and the peak altitude has been reached. As the flight path angle changes, the rocket continues to rotate so that the rocket aligns itself the direction of the oncoming airstream (including the lateral wind velocity), up until the rocket is no longer traveling fast enough to generate a normal force strong enough to force the rocket to continue to rotate, and the rocket rotation angle falls behind the flight path angle (the two curves crossr). The motor burn time is a small portion of the upward flight time, so most of the gravity turn occurs after motor burnout.

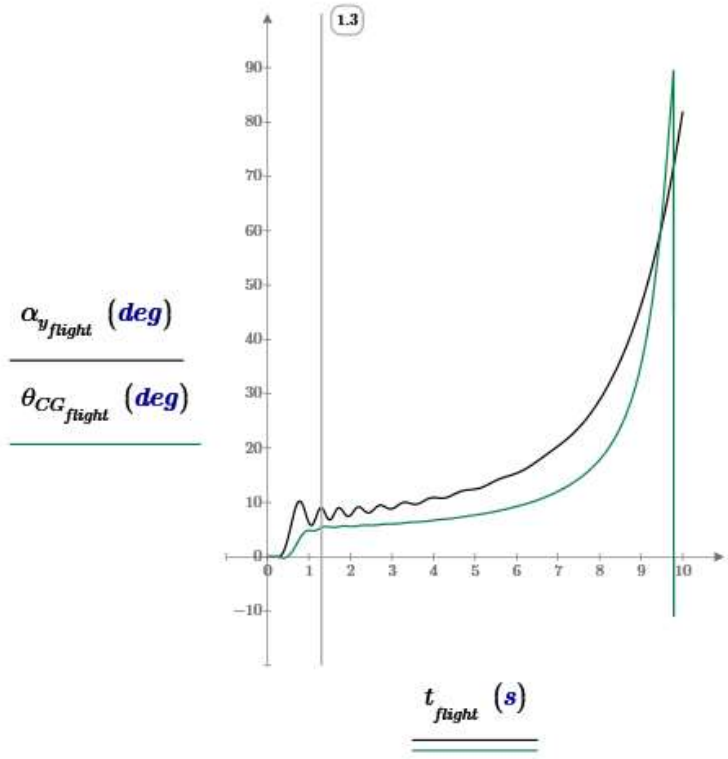

Figure 2-17 Flight trajectory angle (green) and rotation angle (black) for test rocket TR-1 for boost and coast phases

If the rocket never sees a lateral wind, and there is no other rotational perturbation, the rocket will fly straight up to apogee. But once the flight path moves away from vertical, gravity contributes to the continued turn in the flight path.

How much does gravity contribute to the magnitude of the initial turn before motor burnout shown in Figure 2-17? Figure 2-18 shows the complete 2-D model output with the start of the gravity turn on the left, and the 2-D model output with the gravity force in the model set to 0. The comparison of the two graphs shows how much of the turn is due to gravity. Comparing the magnitude of both the rocket rotation and the flight path angle at motor burnout, this shows that a little less than one degree of each turn is due to gravity, so most of the initial step is due to the wind perturbation. The slight droop in the flight path angle in the graph with gravity set to zero is due to the drag force. The drag term's effect is much smaller than that of gravity, and only impacts θ_{CG} .

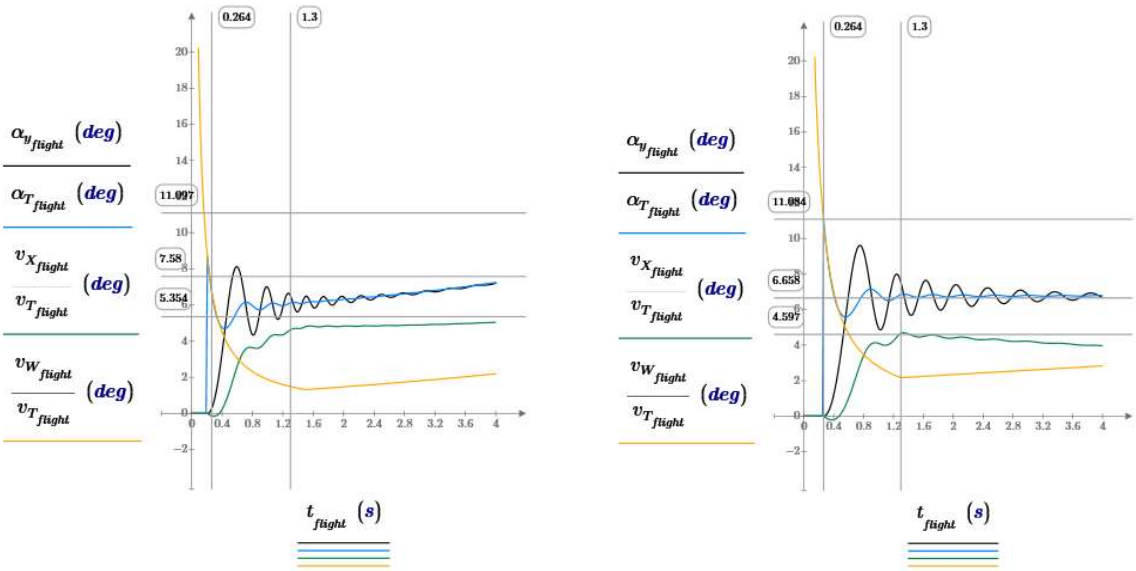

Figure 2-18 Response of TR-1 to a 10 mph step in wind velocity as the rocket leaves the launch guide (0.27 sec) with (left) and without (right) the gravity force

2.4 System Equilibrium

For small rotation angles, the input to the rotational equation, α_T , is the term that provides the coupling between the rotational equation and the X-axis equation of motion[14]

$$\alpha_T = \frac{v_X}{v_T} - \frac{v_w}{v_T}$$

At equilibrium, the angle of attack due to the lateral wind goes to zero, the normal force goes to zero, and the rocket stops rotating, except for the continuation of the gravity turn

$$\alpha_{at}\Big|_{t\to\infty} = 0$$

and the rotation of the rocket aligns with the angle of the oncoming airstream

$$\alpha_y\Big|_{t\to\infty} = \alpha_T$$

[14] (Fetter T. B., 2024, p. 11)

Therefore, at equilibrium

$$\alpha_y\Big|_{t\to\infty} = \frac{v_X}{v_T} - \frac{v_w}{v_T} \tag{2.4-1}$$

This equation does not have a unique solution for the outputs of the system, v_X and α_y. For any value of v_X, a value of α_y exists that satisfies the equation, so a closed form solution for the angle of rotation for a given wind velocity and motor thrust does not exist. The final value of the angle of the rocket's rotation is dependent on the final value of the X-axis velocity, and the final value of the rocket's X-axis velocity is dependent on the final value of the rocket's rotation angle. The values and time where the system reaches equilibrium is dependent on the rate at which the rocket rotates and the rate at which the rocket accelerates along the X-axis. It takes solving the complete system of differential equations to determine what those rates are and what the final equilibrium values are for, v_X and α_y. As described at the beginning of this paper, the final value to the rocket's rotation due to the wind perturbation cannot be determined as a simplified closed form solution and can only be found by solving the complete system of differential equations. And because the differential equations are nonlinear, this requires a numerical solution.

2.5 Rotation After Motor Burnout

All the analyses so far have assumed that the step in wind velocity occurs as the rocket leaves the launch guide, which is normally where the biggest impact due to the wind occurs because of the relatively slow velocity of the rocket as it leaves the launch guide. But what happens if the wind perturbation occurs later in the flight after motor burnout? To examine this case, it is assumed that there is no wind perturbation as the rocket leaves the launch guide, so it is still traveling vertically at motor burnout, shortly after which the wind perturbation occurs.

Figure 2-19 shows the rotational response from the complete model of test rocket TR-1 for a one mile per hour step in wind velocity that occurs at 1.5 seconds into the flight, which is just after motor burnout, when the rocket is traveling at 226 mph. The rocket rotates in response (black trace on the left hand graph) to align itself with the new angle of the total oncoming airstream. The center of gravity of the rocket (green trace on the left hand graph) continues to fly in the same direction it was moving before the step, in this case, straight up, because there is no component of thrust to accelerate the rocket along the X-axis. Therefore, the angle of the direction of the flight path of the center of gravity, θ_{CG}, remains unchanged when the wind step occurs after motor burnout.

The size of the rotation angle is the ratio of the wind velocity to the total velocity of the oncoming airstream at 1.5 sec

$$\alpha_T = \left.\frac{v_w}{v_T}\right|_{t_{step}} = 0.253\,\text{deg}$$

and, since the flight path angle is zero,

$$\Delta = \alpha_T$$

The slight drift in the flight path angle after the step is due to the drag term in the X-axis equation of motion. Because the rocket angle of attack has a slight negative average due to its phasing (short positive quarter cycle followed by a half negative cycle), the drag term causes a small negative X-axis velocity which causes the small negative drift in the flight path angle. The X-axis side-to-side motion continues after motor burnout because the motion is due to the lift force, so the enhanced damping also continues after motor burnout due to the coupling between the X-axis equation of motion and the rotational dynamics equation[15].

[15] (Fetter T. B., 2024, p. 16)

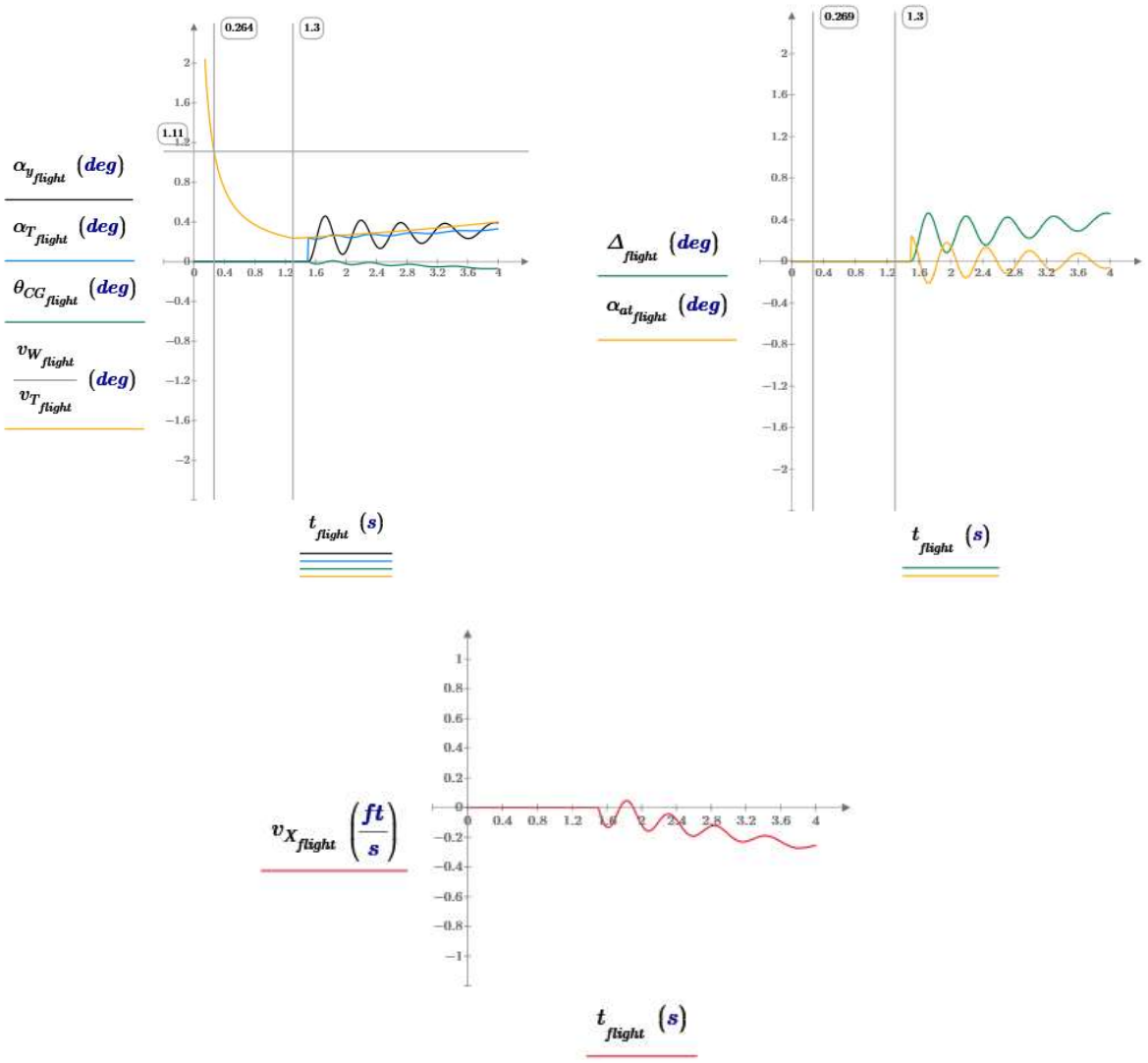

Figure 2-19 Response of TR-1 to a 1 mph step in wind velocity at 1.5 sec, after motor burn out (1.3 sec)

2.6 Angle of Rotation Sensitivity Analyses

What impact does the design of a rocket have on its propensity to rotate into the wind? Since a closed form solution for the magnitude of the rocket's rotation into the wind does not exist, a series of sensitivity analyses must be used to evaluate the rotational angle and flight path sensitivities to changes in the rocket design parameters. For each sensitivity graph, a design parameter is changed over a range of values, and the complete flight model is then run to

determine the rocket's rotation and flight path angles for each value of that design parameter. The resulting graph shows the rotation angle and flight path angle versus the design parameter as it is varied about a nominal value.

To determine the magnitude of the rotation angle and the flight path angle, a single value for the magnitude of the rotational step response must be chosen. The average value of the step response at motor burnout is the value used here as shown in Figure 2-20. By this time, the initial wind-caused rotation is complete, and the contribution of gravity is still small, so this is a good representation of the size of the initial turn due to the wind perturbation.

To determine this angle, a line is first fit to the complete flight model step response for those two angles, as shown in Figure 2-20. The line is fit to the data over a range starting at motor burnout and ending 4 seconds into the flight. Within that range, the step has completed and the impact of the gravity turn is still minimal. The time is long compared to the frequency of the ringing, so a center value of the damped oscillation can be determined. The value that is used for the sensitivity analysis is the value of the best fit line at the time of motor burn out.

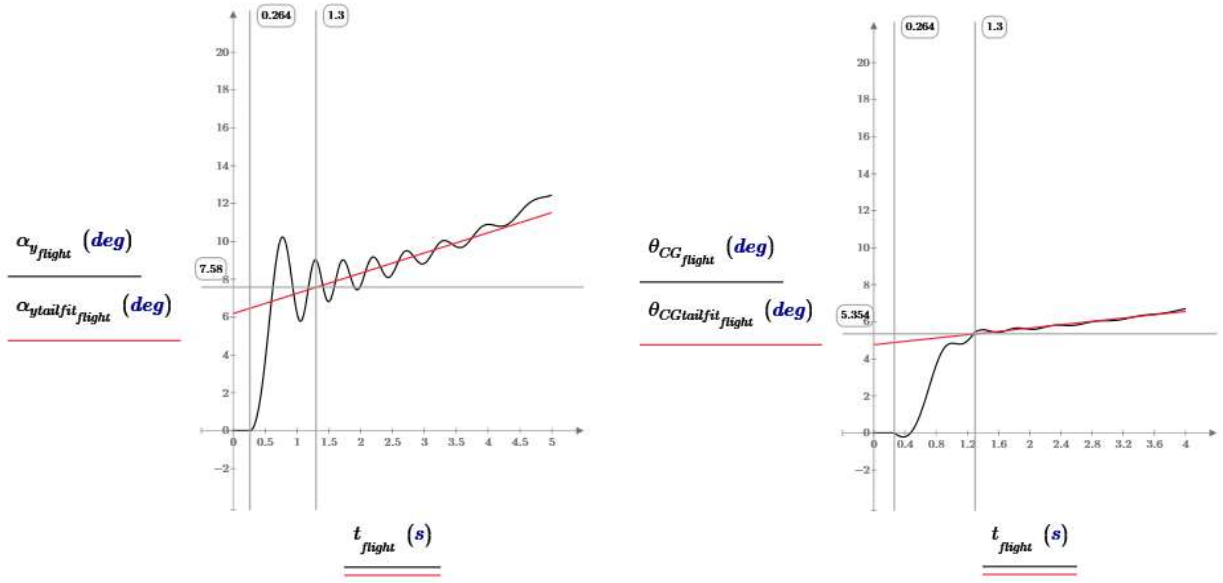

Figure 2-20 Line fit for determining the angle of rotation and flight angles

The first sensitivity figure, Figure 2-21 , shows the rotational sensitivity to the wind velocity. The step response of the rocket rotation angle and the flight path angle are both linear functions of the velocity of the wind that occurs as the rocket is leaving the launch guide. The frequency of oscillation and the damping ratio are constant over the

range of wind velocities[16]. Because the flight path angle increases with increasing wind velocity, the maximum altitude decreases with increasing wind velocity. Also, the larger the initial wind induced angle of the flight path, the earlier in the flight the gravity turn starts to have a significant impact on the flight path angle.

[16] (Fetter T. B., 2024, p. 11)

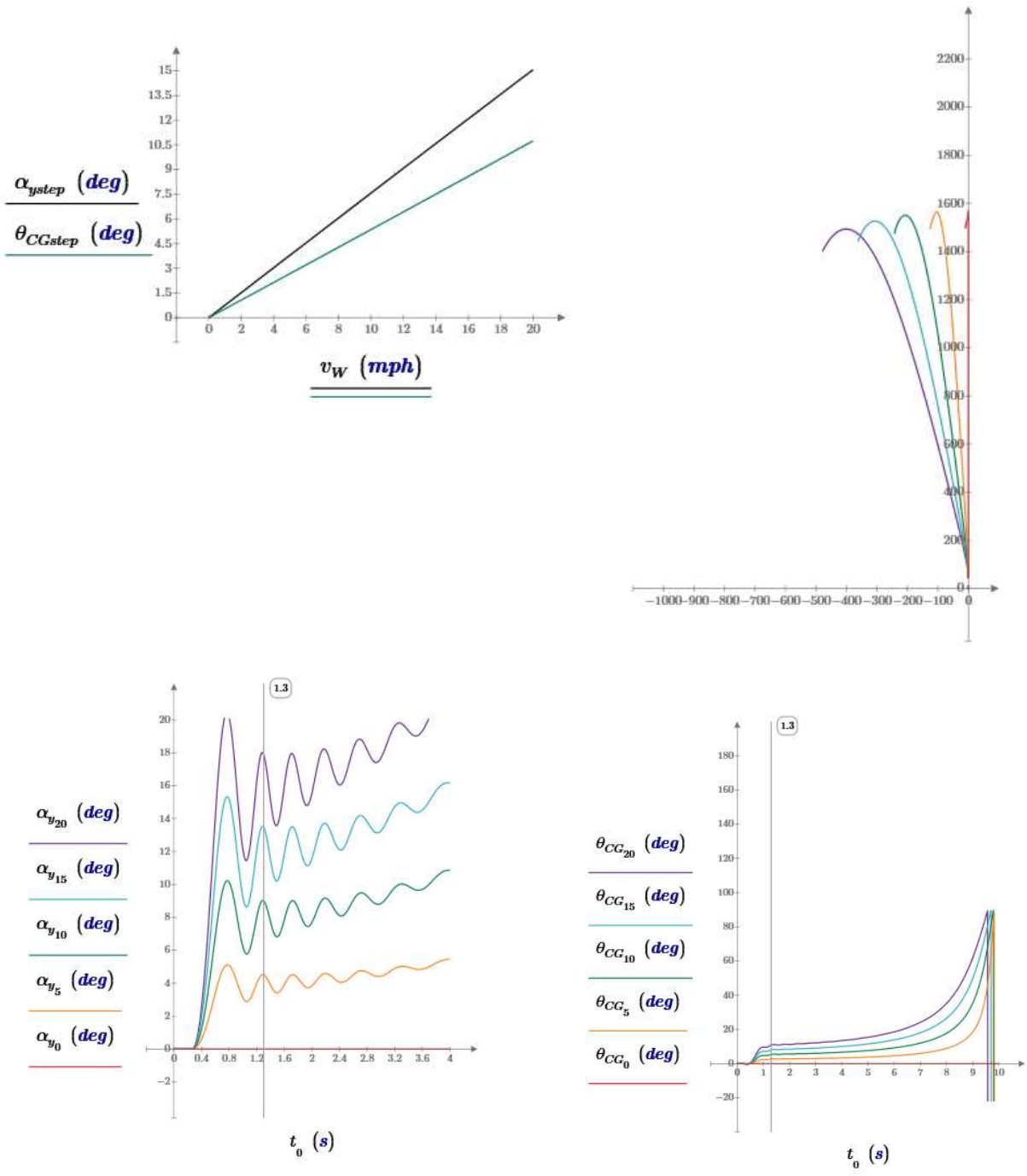

red	orange	green	blue	violet
0 mph	5 mph	10 mph	15 mph	20 mph

Figure 2-21 Rotation parameters sensitivity to wind velocity

The following figures, Figure 2-22 to Figure 2-25, show the sensitivities of the rotational parameters to the key rocket design parameters, including the fin size, body tube length, nose weight mass, and the density of the rocket construction material. All the graphs are calculated using the component parameters from test rocket TR-1 except for the one parameter that is being varied about its nominal value from TR-1. Each graph indicates the nominal parameter value for TR-1 which has a 2.6 caliber stability margin at motor burnout.

Since TR-1 starts with a 2.6 caliber stability margin, a negative value of nose weight mass, which is possible in a simulation, is used to give a sensitivity range that covers lower values of stability margin. The fin scaling sensitivity, k, is a linear scaling factor for the size of the fin, with a value of 1 being the nominal size of TR-1's fins. The material density sensitivity assumes the rocket is constructed from material all the same density. The range of densities includes the range from paper and balsa up through epoxy/fiberglass. For the TR-1 design, it is not possible to get to one caliber of stability margin by just varying the material density, using a reasonable range of material densities.

For each figure, the first graph shows the rocket rotational angle and the flight path angle versus the design parameter. The graph below the angle sensitivity graph shows the stability margin (the distance between the center of pressure and the center of gravity) sensitivity. Even though it has been shown that the rotational dynamic stability does not directly correlate to the stability margin[17], the term "stability margin" is still used here for the distance between the center of pressure and center of gravity because of its common usage in the rocketry community. For both the angle sensitivity graph and the stability margin sensitivity graph, the right hand vertical marker is the nominal value for that parameter for test rocket TR-1. That parameter is then varied over a range that is less than and greater than its nominal value. The left hand vertical marker is the sensitivity parameter value that gives 1 caliber of stability margin as can be seen on the stability margin graph. The useful range of the sensitivity parameter for a stable rocket is to the right of this line since a stability margin of less than 1 caliber is not recommended to ensure stability. The graph on the top right shows the flight profile for five discrete sensitivity parameter values listed in the key table. The bottom two graphs show the individual step responses for the angle of rotation and the flight trajectory angles.

Figure 2-22 shows the sensitivity to body tube length. Above about 1.2 ft length needed for 1 caliber of stability margin, the rotation and flight path angles change very little, even though the stability margin varies over a large range.

Figure 2-23 shows the sensitivity to the nose weight mass. The rotation and flight path angles are more sensitive to increasing the nose weight mass than they are to increasing the body tube length.

[17] (Fetter T. B., 2024)

Figure 2-24 shows the sensitivity to the fin size. The rotation and flight path angles are most sensitive to the change in relative fin size within a reasonable range of values for each design parameter.

Figure 2-25 shows the sensitivity to the material density. There is very little change in the rotation and fight path angles with the change in the material density, but there is a large change in the rise time of both the rocket rotation angle and flight path angle.

These graphs show that some of the rocket design parameters have a greater impact on the rotational and flight path angles than others, but that impact is not directly correlated to the stability margin (distance between the center of pressure and center of gravity).

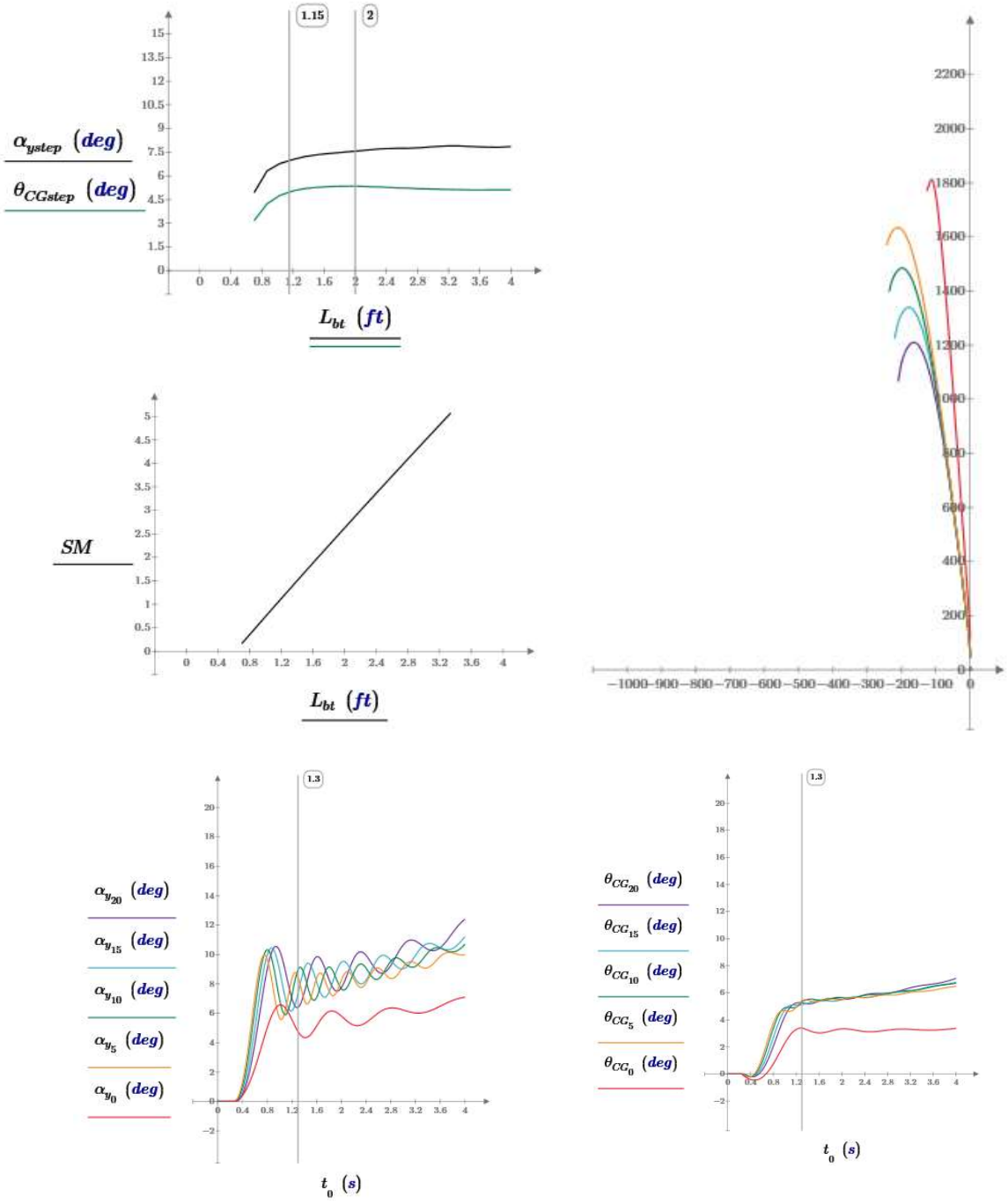

Trace	red	orange	green	blue	vilot
BT Length	0.7 ft	1.25 ft	2.35 ft	3.175 ft	4.0 ft

Figure 2-22 Rotation parameters sensitivity to body tube length

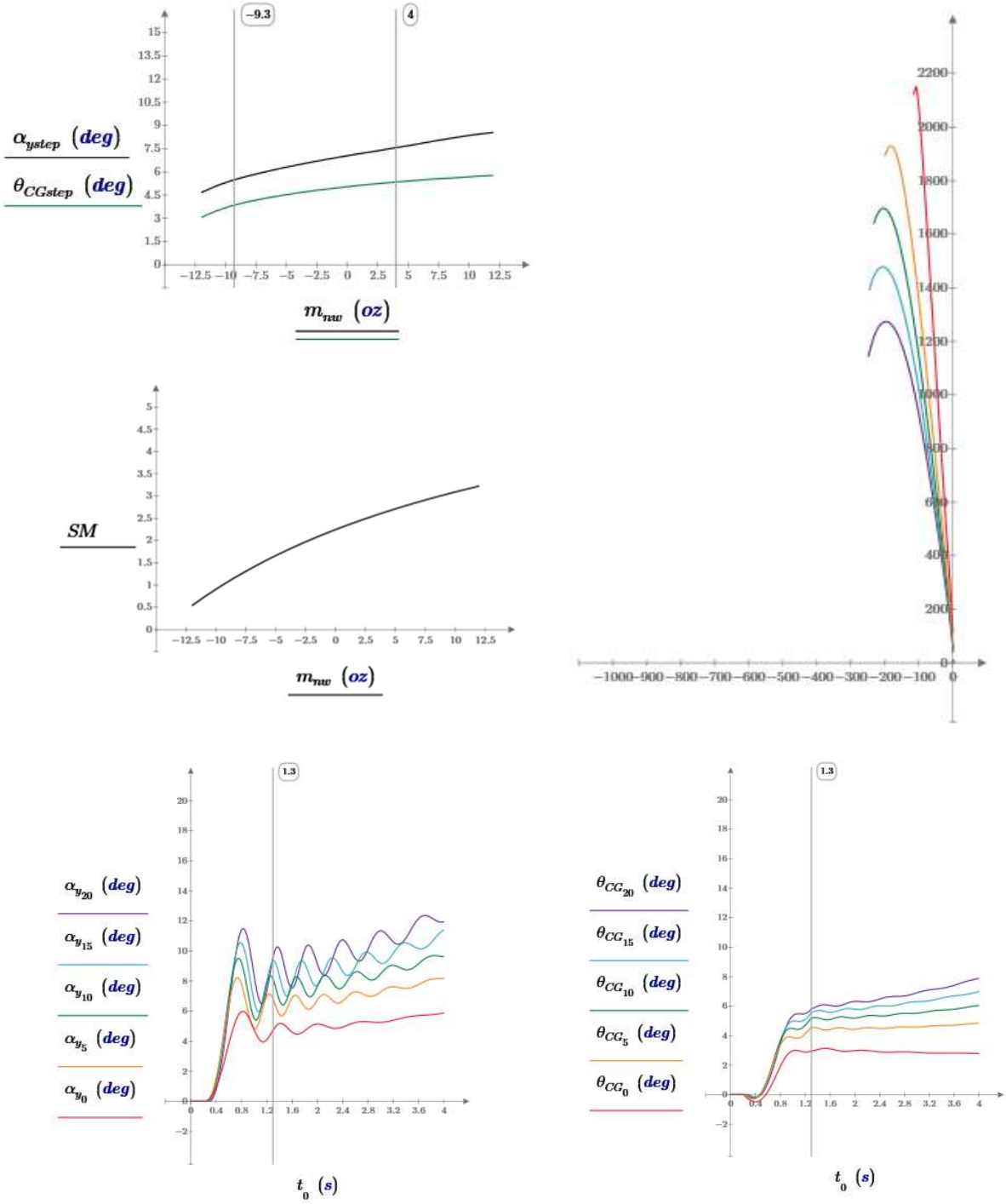

Trace	red	orange	green	blue	violet
Nose Mass	-12 oz	-6 oz	0 oz	6 oz	12 oz

Figure 2-23 Rotation parameters sensitivity to nose weight mass

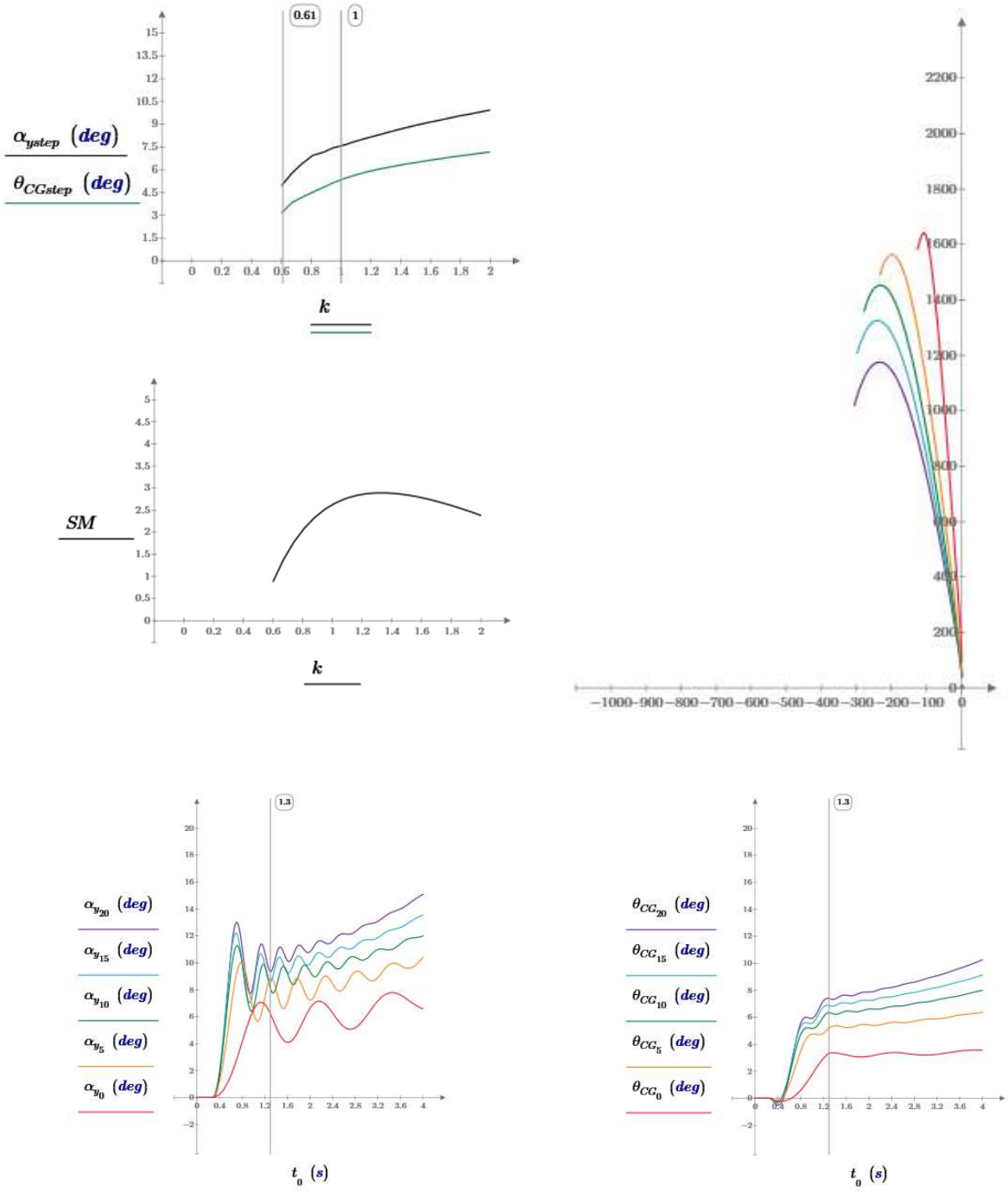

Trace	red	orange	green	blue	violet
Fin Size	0.67	0.95	1.3	1.65	2.0

Figure 2-24 Rotation parameters sensitivity to fin size

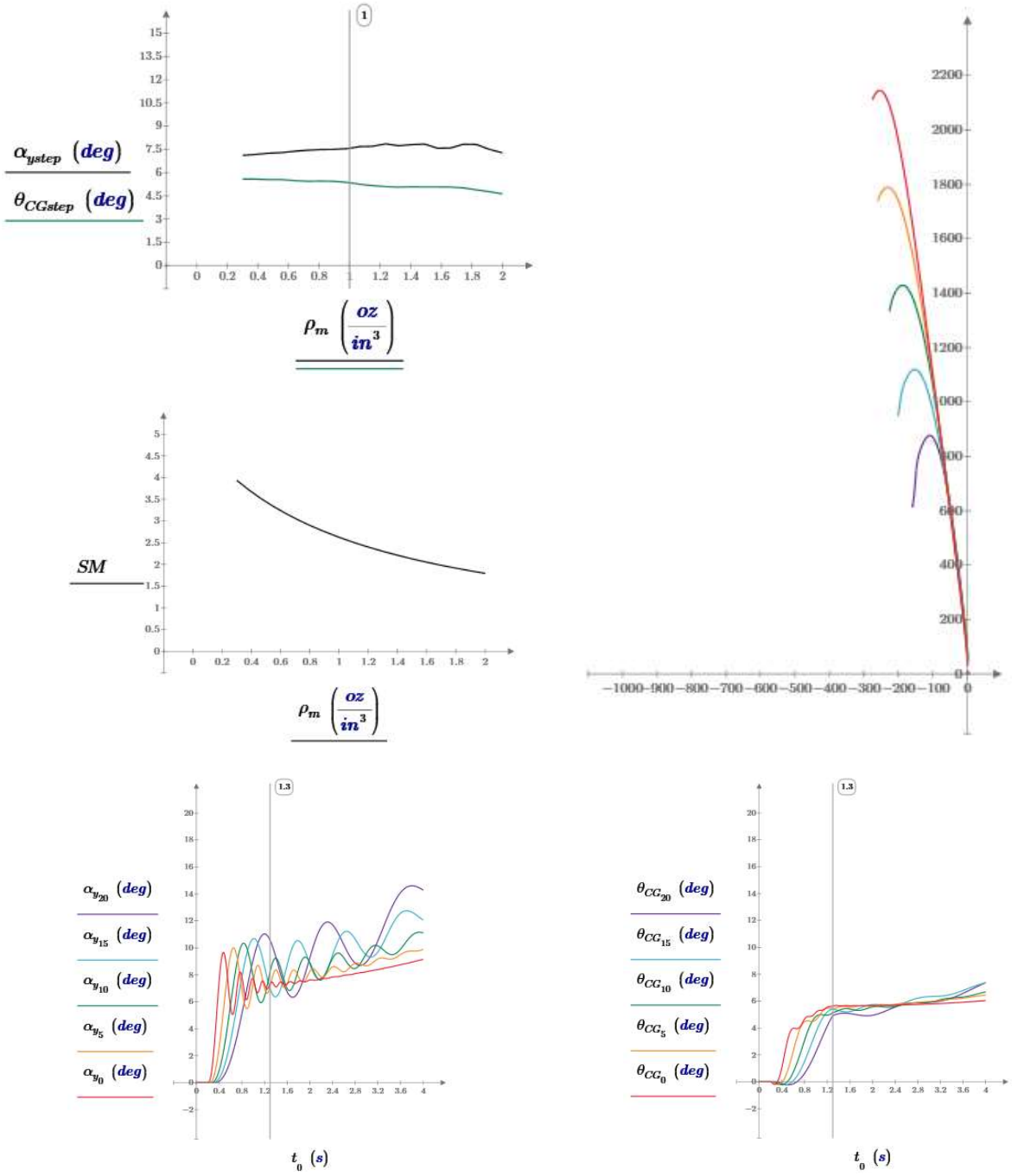

Trace	red	orange	green	blue	violet
Density	0.3 oz/in^3	0.725 oz/in^3	1.15 oz/in^3	1.575 oz/in^3	2.0 oz/in^3

Figure 2-25 Rotation parameters sensitivity to material density

All the flight trajectories in the previous figures show that the maximum altitude decreases as the sensitivity parameter value increases. Figure 2-26 shows that the total mass of the rocket increases significantly with the increase in all the sensitivity parameters, as would be expected. The increasing total mass will have a significant impact on the maximum altitude of the rocket, but it is not clear how much of the reduction in maximum altitude is due to the increased mass and how much is due to the increase in the flight path angle.

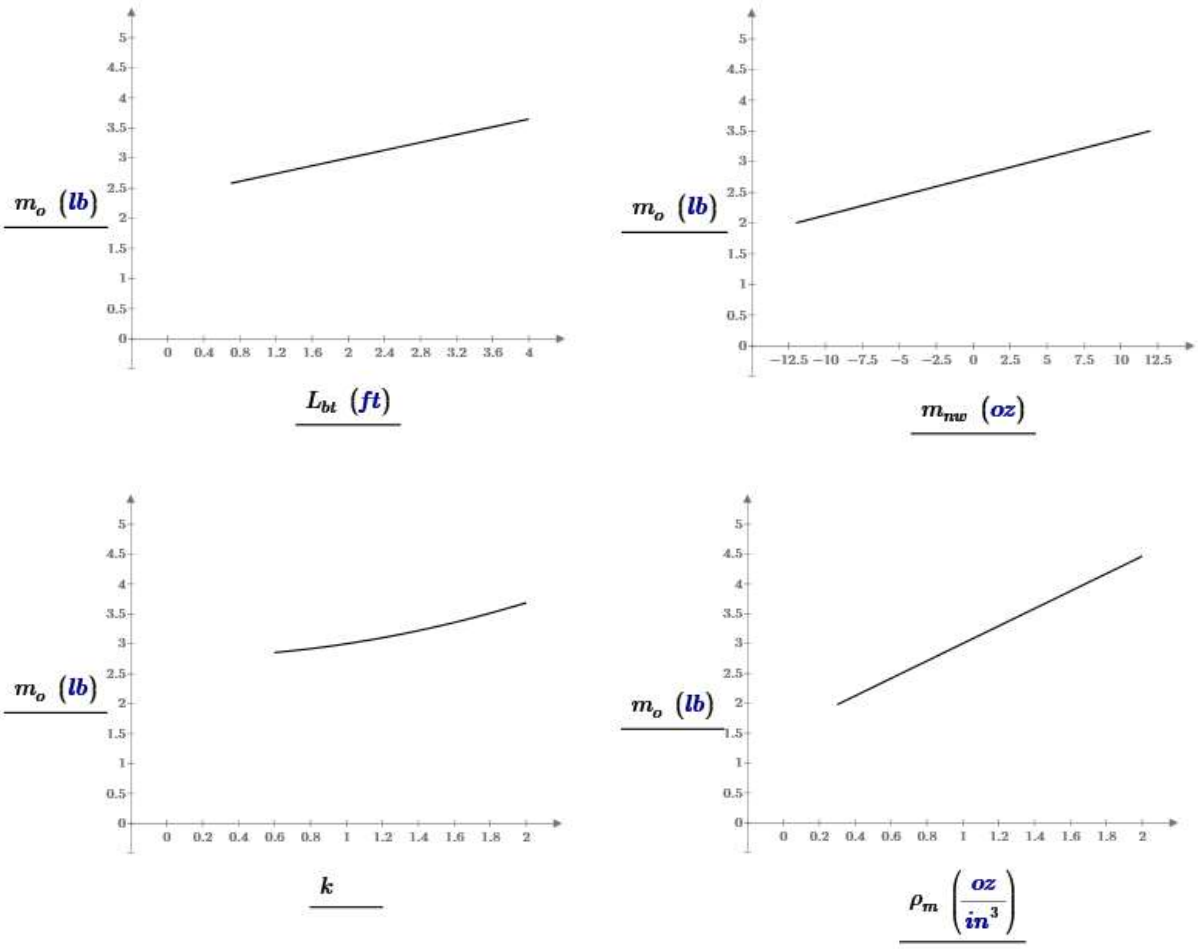

Figure 2-26 Total mass of the rocket vs sensitivity parameter

To determine how much of the altitude loss is due to the change in the mass, and how much is due to the change in the flight path angle, a series of three flights can be simulated where the parameters for each flight can be set to distinguish between the impact of the mass versus the impact of the flight path angle.

Figure 2-27 shows a series of three flights where the body tube length is the sensitivity parameter being tested. For the first flight, test rocket TR-1 is simulated with a 1 ft body tube length using material density of 1 oz/in^3, the density of fiberglass. For the second flight, the body tube length is increased to 2 ft, which increases the total mass of the rocket from 2.7 lb for the first flight to 3.3 lb for the second flight. The resulting peak altitude drops almost 400 ft. The angle of the flight path also increases slightly due to the increase in the body tube length. For the third flight, body tube length is kept at 2 ft, but the density of the material is reduced to .63 oz/in^3 to reduce the total mass of the rocket back to the total mass of the rocket of the first flight with the 1 ft body tube. The result is a peak altitude that is close to the peak altitude of the first flight with the shorter body tube but with the flight path angle similar to the flight path angle of the second flight with the longer body tube. This is because the density of the material has very little impact on the flight path angle. This shows that the reduction in the altitude is due almost entirely to the increase in the total mass of the rocket and not due to the change in the flight path angle due to the longer body tube.

Figure 2-28 and Figure 2-29 show that the same is true for varying both the nose weight mass and the fin size. In all three cases, the change in the total mass of the rocket is the cause of most of the reduction and the maximum altitude of the rocket, not the change in the flight path angle. The flight path angle graph in Figure 2-29 shows that the change in the flight path angle for the fin size scenario is about 1.7 deg, the largest of the three scenarios.

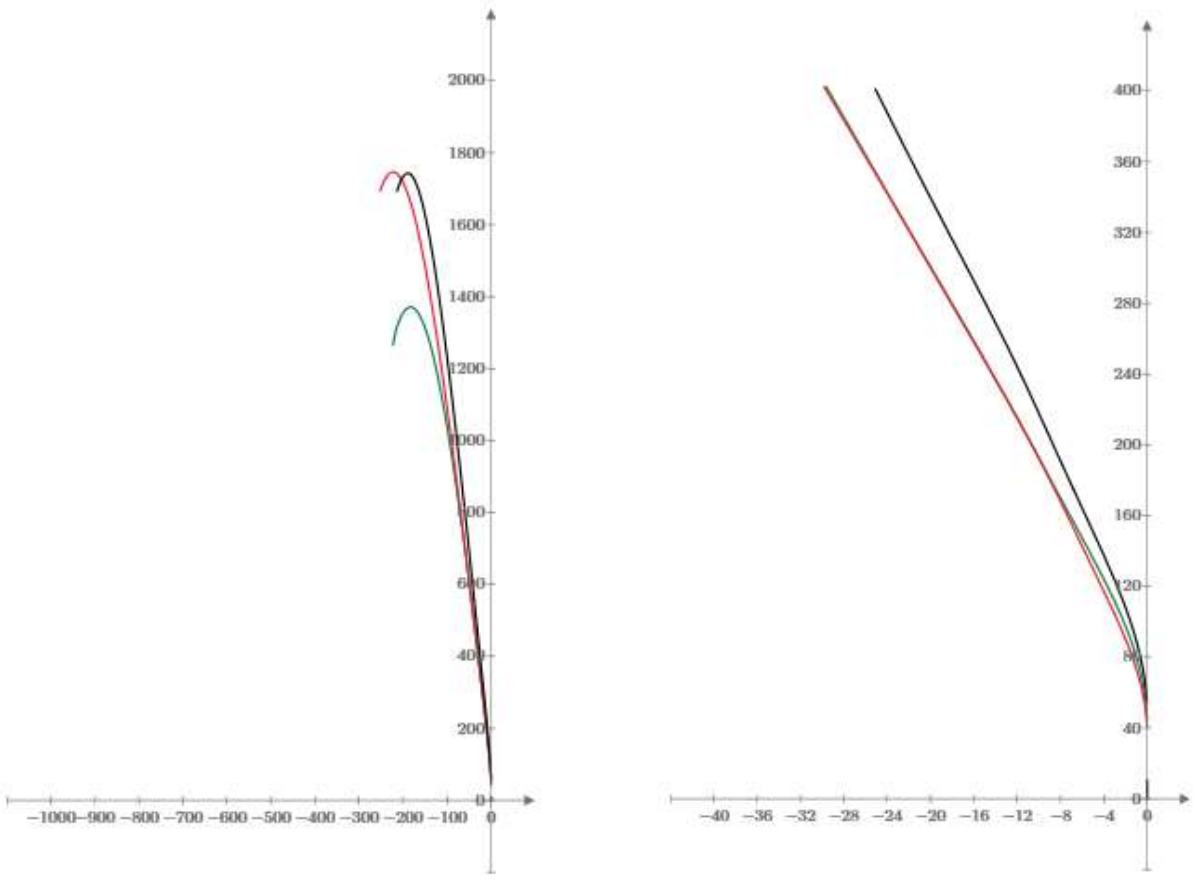

Flight	Trace	Body Tube	Material Density	Mass	Stability Margin
1	Black	1 ft	1 oz/in^3	2.7 lb	0.7
2	Green	3 ft	1 oz/in^3	3.3 lb	4.5
3	Red	3 ft	0.63 oz/in^3	2.7 lb	5.3

Figure 2-27 Changing body tube length while adjusting material density to maintain total mass

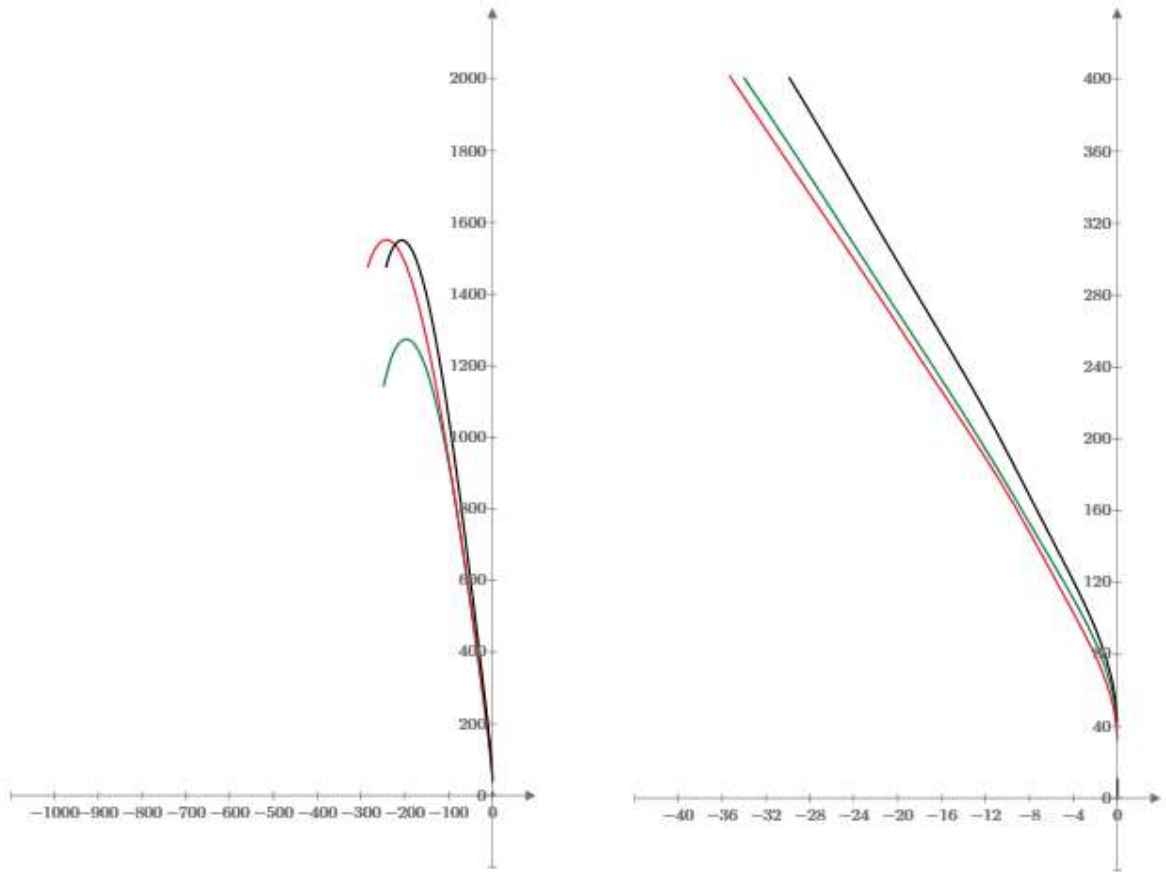

Flight	Trace	Nose Weight Mass	Material Density	Mass	Stability Margin
1	Black	4 oz	1 oz/in^3	3.0 lbs	2.6
2	Green	12 oz	1 oz/in^3	3.5 lbs	3.2
3	Red	12 oz	0.65 oz/in^3	3.0 lbs	3.8

Figure 2-28 Changing nose weight mass while adjusting material density to maintain total mass

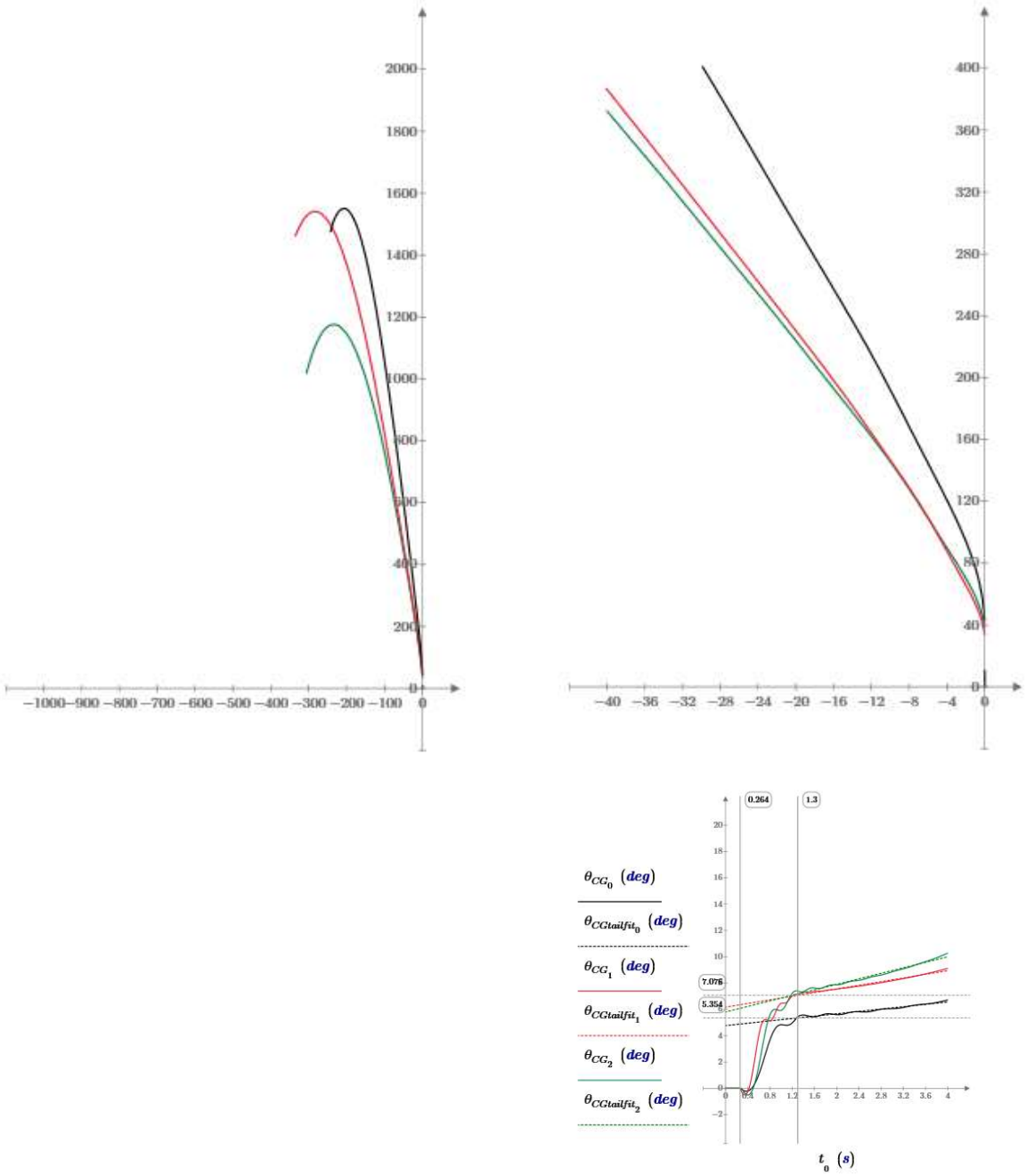

Flight	Index	Fin Size	Material Density	Mass	Stability Margin
1	Black	1x	1 oz/in^3	3.0 lb	2.6
2	Green	2x	1 oz/in^3	3.7 lb	2.4
3	Red	2x	0.68 oz/in^3	3.0 lb	2.9

Figure 2-29 Changing fin size while adjusting material density to maintain total mass

Figure 2-30 shows the initial fight path angle required to match the reduction in maximum altitude due to a change in the mass of the rocket. For the first fight, test rocket TR-1 is simulated with a material density of .63 oz/in^3. For the second flight, the material density is increased to 1 oz/in^3, and the maximum altitude drops as the mass of the rocket increases from 2.5 lb to 3.0 lb. For the third flight, the material density is changed back to the lighter .63 oz/in^3 density, and the initial launch angle is increased until the maximum altitude equals the maximum altitude of the second flight with the denser material. The resulting launch angle 19°, which is significantly greater than the approximately 2° increase in the fight path angle seen in the prior 3 scenarios. This shows it takes a significant initial flight path angle to match the reduction and the maximum altitude seeing in each of these scenarios due to the increase in the mass of the rocket.

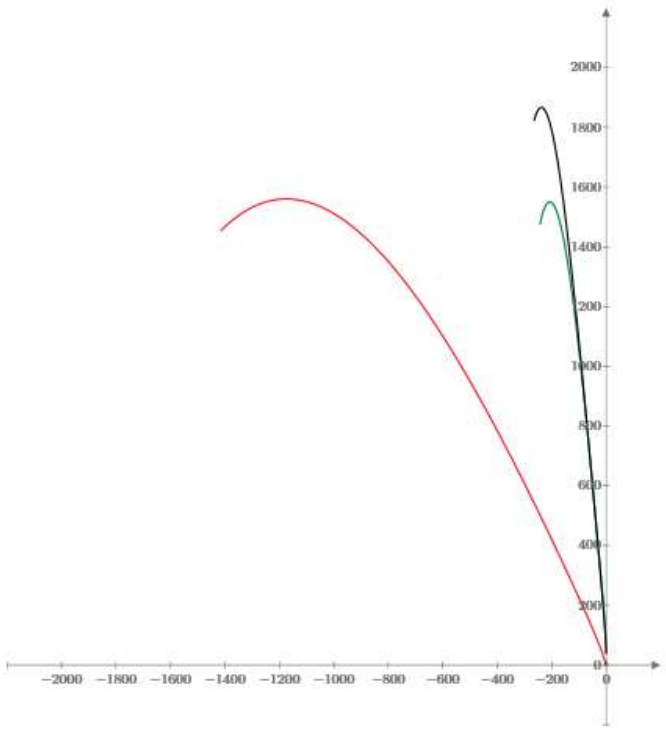

Flight	Trace	Initial Launch Angle	Material Density	Mass	Stability Margin
1	Black	0 deg	0.63 oz/in^3	2.5 lbs	3.2
2	Green	0 deg	1.0 oz/in^3	3.0 lbs	2.6
3	Red	19 deg	0.63 oz/in^3	2.5 lbs	3.2

Figure 2-30 Initial launch angle needed to match the maximum altitude of the heavier rocket

Figure 2-31 shows the rotational sensitivity to motor burn time for test rocket TR-1 nominally flying an H128W motor with a 10 mph wind. In this case, no rocket parameters are varied. The total impulse of the motor is kept constant, so the average thrust increases with decreasing burn time. Both the rocket rotation angle and the flight path angle are very sensitive to motor burn time compared to the other sensitivity studies, within the reasonable range for each of these parameters used for the sensitivity studies. The lower velocity of the rocket as the rocket leaves the launch guide with increasing burn time significantly increases the initial angle of the oncoming airstream, which increases the rotation of the rocket and its flight path. Although a higher velocity causes increased drag

which can negatively impact the maximum altitude, in this case, the maximum velocity produced by the H128W motor is not enough to outweigh the increase in maximum altitude due to the decrease in rotation of the rocket.

If the rotation of the rocket does not complete before motor burnout, the increase in the flight path angle would stop before the rocket rotation completes. Figure 2-32 shows the rocket rotation and flight path angles for the burn time sensitivity analysis based on the H128W motor. It shows that the rotation rate increases with faster burn times so that the rotation always completes before motor burnout, even for the fastest burn times shown. This is because the faster burn time flights leave the launch guide at larger velocities and the natural frequency increases with the larger velocity, which leads to a faster rotational rise time.

Figure 2-33 shows the flight paths for test rocket TR-1 flying a larger I200W motor while varying the burn time of the motor keeping the total impulse constant, and a 10 mph wind. The total impulse of the I200W motor is large enough to cause velocities that are high enough that drag starts to significantly impact the maximum altitude of the flight. For the shortest two burn times, the maximum altitude drops due to the increased drag term which is proportional to the square of the velocity. The 1.75 second burn time is the optimal burn time, balancing the velocity needed to reduce the turn into the wind and the altitude loss due to drag. The longest two burn times then see a reduction in the maximum altitude due to the greater turn into the wind.

Figure 2-34 shows the flight paths for test rocket TR-1 flying the same larger I200W motor while varying the burn time of the motor keeping the total impulse constant, but with a 1 mph wind. With the lower wind speed, the slower burn times all increase the maximum altitude because the loss in maximum altitude due to the wind is less than the loss in altitude due to the drag for all burn times, and the slowest burn time has the least drag. This shows that the optimal burn time is slower the lower the wind velocity. For zero wind, the longest burn time would always result in the highest maximum altitude up until the point where the rocket velocity is so slow that gravity starts to play a role in determining the maximum altitude (if the thrust were less than 1 g, the rocket would never get off the ground).

The lower the wind velocity the longer the optimal burn time will be. The stronger the wind the shorter the optimal burn time will be. But for many fights where the motor size is too small to reach velocities where drag has a significant impact on the maximum altitude, the shortest burn time (within the range of burn times available in commercial motors) will always give the maximum altitude when there is a nonzero wind velocity.

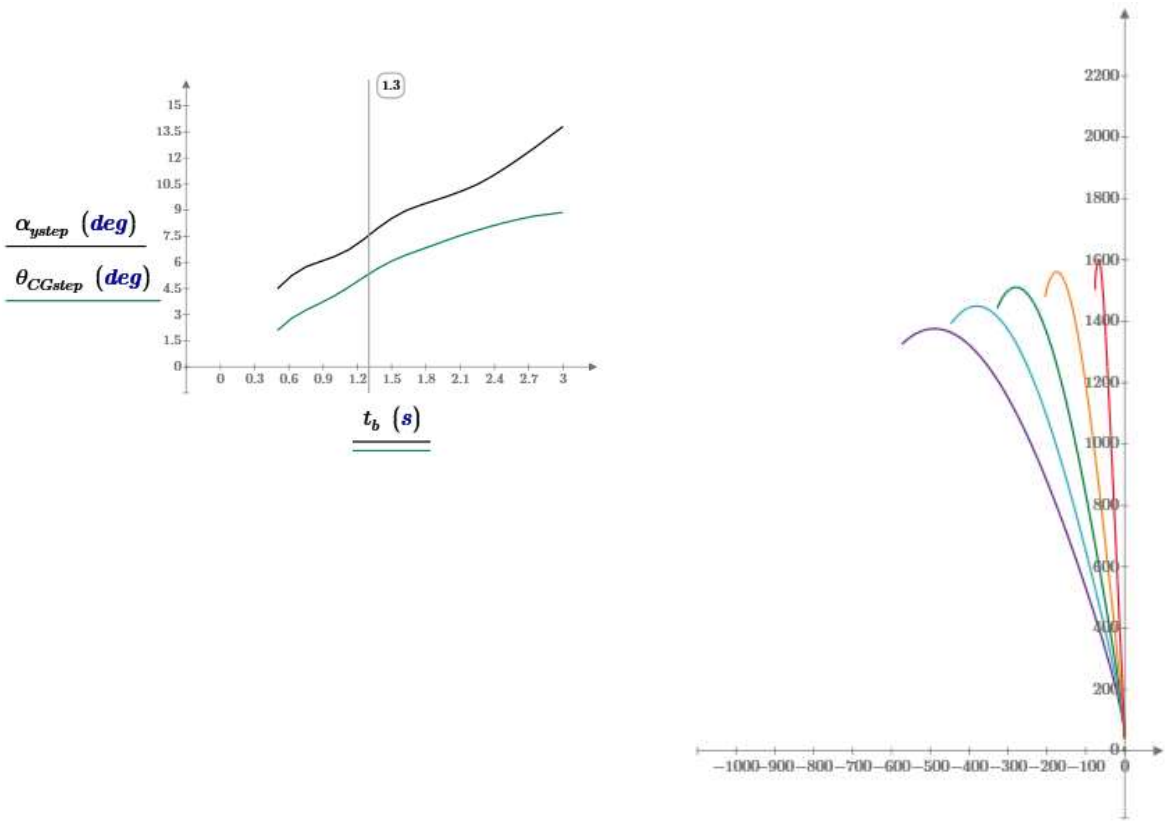

Trace	Burn Time
red	0.5 s
orange	1.125 s
green	1.75 s
blue	2.375 s
violet	3.0 s

Figure 2-31 Sensitivity to burn time for TR-1 flying on an H128W in a 10 mph wind

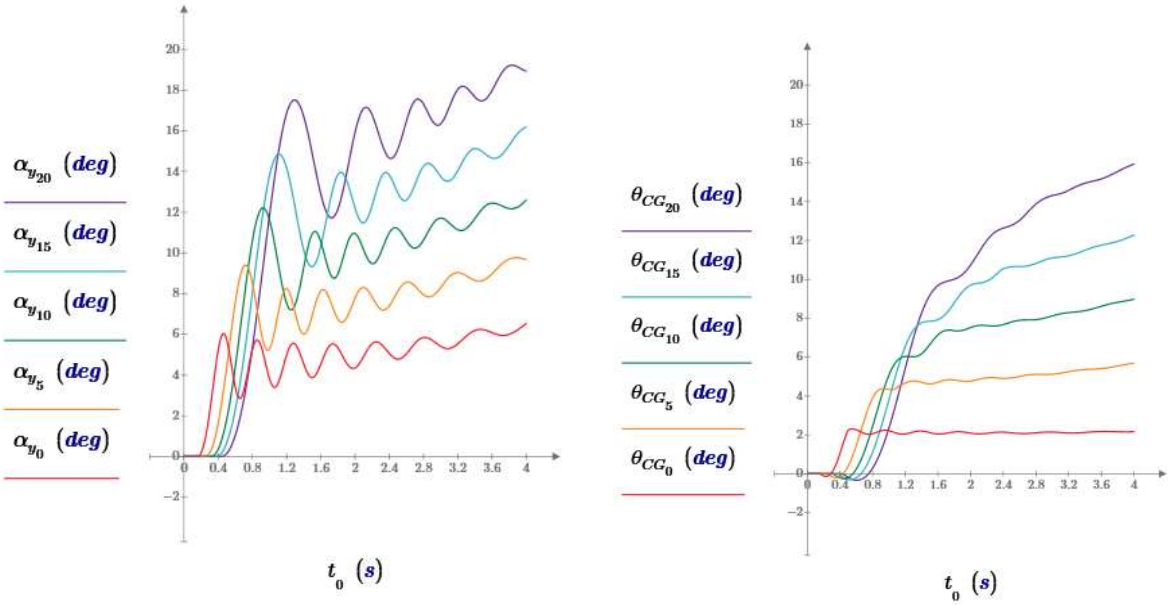

Trace	Burn Time
red	0.5 s
orange	1.125 s
green	1.75 s
blue	2.375 s
violet	3.0 s

Figure 2-32 Rocket rotation and flight path angles for the burn time sensitivity analysis based on the H128W motor

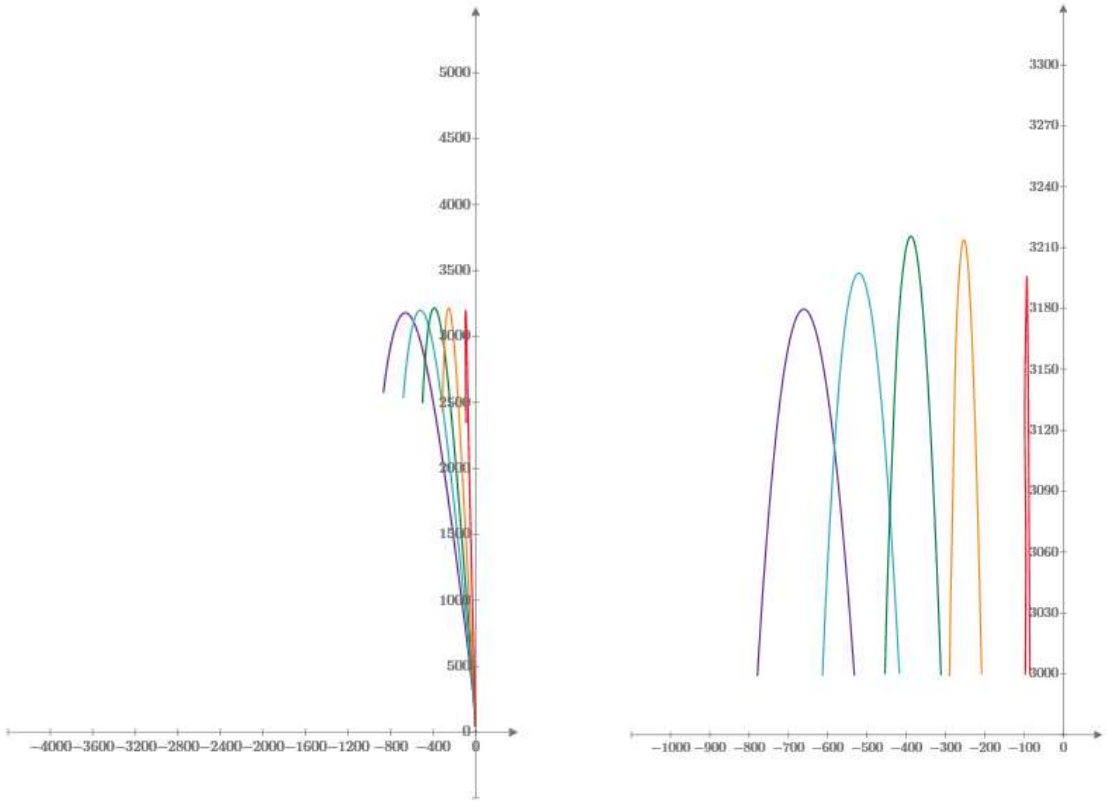

Trace	Burn Time	
red	0.5 s	Altitude loss due to higher velocity drag
orange	1.125 s	
green	1.75 s	Optimal burn time
blue	2.375 s	Altitude loss due to greater rotation
violet	3.0 s	

Figure 2-33 Flight paths vs. burn time for TR-1 flying on an I200W in a 10 mph wind

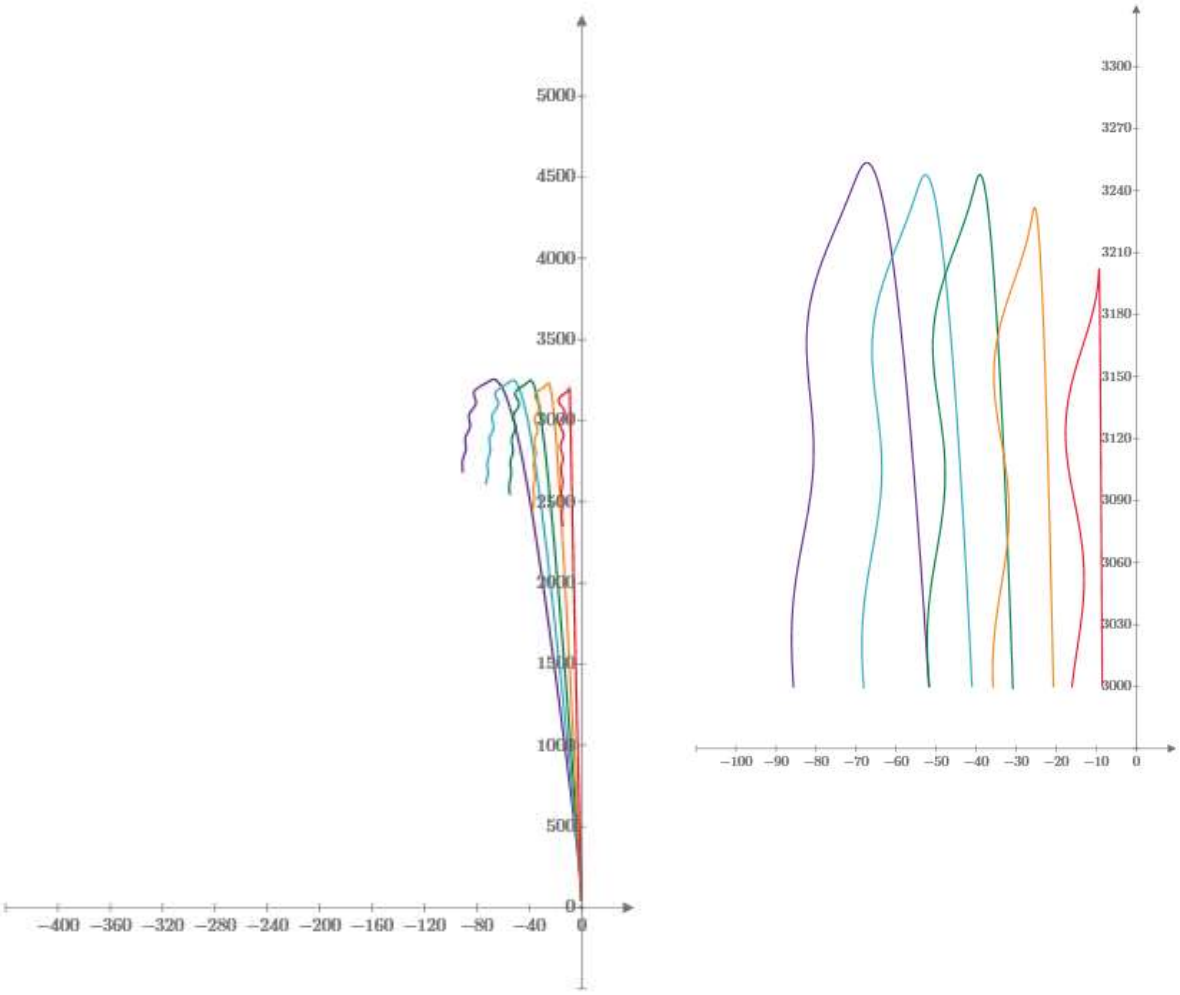

Trace	Burn Time
red	0.5 s
orange	1.125 s
green	1.75 s
blue	2.375 s
violet	3.0 s

Figure 2-34 Flight paths vs. burn time for TR-1 flying on an I200W in a 1 mph wind

3 Flight Data

3.1 Test Rocket TR-1

Test rocket TR-1 was designed and built with the purpose of gathering flight data to test the models presented in the Rotational Dynamic Stability paper[18], but was used to gather data for this paper as well. The TR-1 design parameters needed for the flight model are given in Table 3-1.

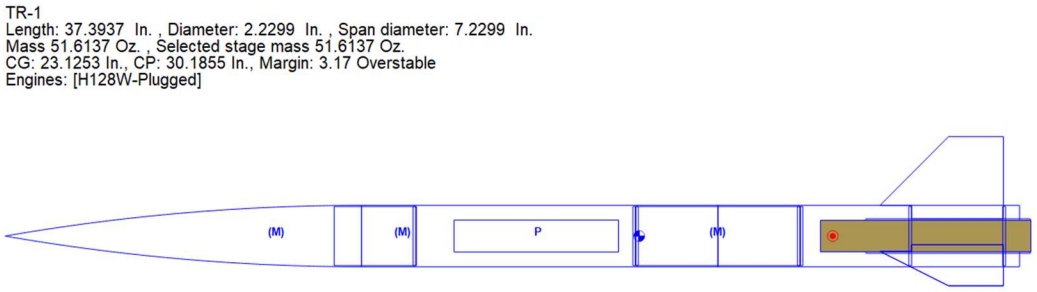

Figure 3-1 TR-1 test rocket

Rocket diameter	D_r = 2.27 in	Motor	AT-H128W
Nosecone length	L_{nc} = 13 in	Motor length	L_m = 7.25 in
Nosecone thickness	T_{nc} = .125 in	Motor mass	m_m = .454 lb.
Nosecone density	ρ_{nc} = 1.0 oz/in^3	Motor propellant mass	m_p = .207 lb.
Nose weight	m_{nw} = 4 oz	Motor burn time	t_b = 1.3 sec
Body tube length	L_{bt} = 24 in	Motor total impulse	I_t = 172.9 N sec
Fin root edge length	c_r = 4.5 in	Launch guide length	l_{lr} = 10 ft
Fin tip edge length	c_t = 2 in	Rocket total length	L_{ne} = 37 in

[18] (Fetter T. B., 2024)

Fin span from body	s = 2.5 in	Rocket total mass	m_o = 3.21 lb.
Fin mid cord sweep ang	Γ_c = 26.6 deg	Center of gravity	L_{CG} = 22.89 in
Fin thickness	T_f = .15 in	Center of pressure	L_{CP} = 28.4 in
Fin density	ρ_f = 1.0 oz/in^3	Stability Margin	SM = 2.42
Number of fins	N = 3	Rocket moment of inertia	I_L = 3.071 lb ft^2
Motor tube length	L_{mt} = 6 in	Rocket drag coefficient	C_D = .8
Motor tube diameter	D_{mt} = 1.269 in	Normal force coefficient	$C_{N\alpha}$ = 10.2
Motor tube thickness	T_{mt} = .062 in	Rocket lift coefficient	$C_{L\alpha}$ = 10.2
Motor tube density	ρ_{mt} = 1.0 oz/in^3	Natural frequency	ω_n = 0.49 Hz @ 50.9 mph
Motor mount length	L_{mm} = 0.188 in	Natural frequency	ω_n = 1.05 Hz @ 110 mph
MM density	ρ_{pw} = 1.0 oz/in^3	Natural frequency	ω_n = 2.24 Hz @ 227 mph
Parachute/ebay mass	m_{par} = 16.7 oz	Uncoupled damping ratio	ζ = 0.0105
Parachute length	L_{par} = 4 in	Coupled damping ratio	ζ' = 0.0539

Table 3-1 TR-1 model parameters

The purpose of the flight instrumentation was to measure the rocket's rotation about its three axes and its side-to-side motion. The rotation rate and acceleration of the rocket was measured using an RAF Datalogger[19]. The Datalogger has two 3-axis accelerometers and one 3-axis rate gyroscope. The Datalogger logs the data to an onboard micro-SD card which is downloaded into a Mathcad worksheet or an Excel spreadsheet where it is analyzed, and the flight graphs are generated. The data sample rate for the Datalogger is 0.75 ms, but the data is decimated to a 7.5 ms sample rate using a Python script to reduce computation times before loading into a Mathcad worksheet for analysis.

Figure 3-2 RAF Datalogger

[19] (Feretich, 2015-2018)

Since the Datalogger measures the rotational rate of the rocket's three axes in the rocket frame of reference, the orientation of the rocket in the ground-based frame of reference must be determined by doing a frame of reference axis translation using Euler's angles[20]. This is done as a part of the post flight data analysis.

The TR-1 electronics bay, which contains an Altus Metrum Easy Mini barometric deployment altimeter and the RAF Datalogger, is located rearward in the rocket, just ahead of the motor, to locate the accelerometers as close to the rocket's center of gravity as possible. A Beeline GPS is flown in the nosecone compartment.

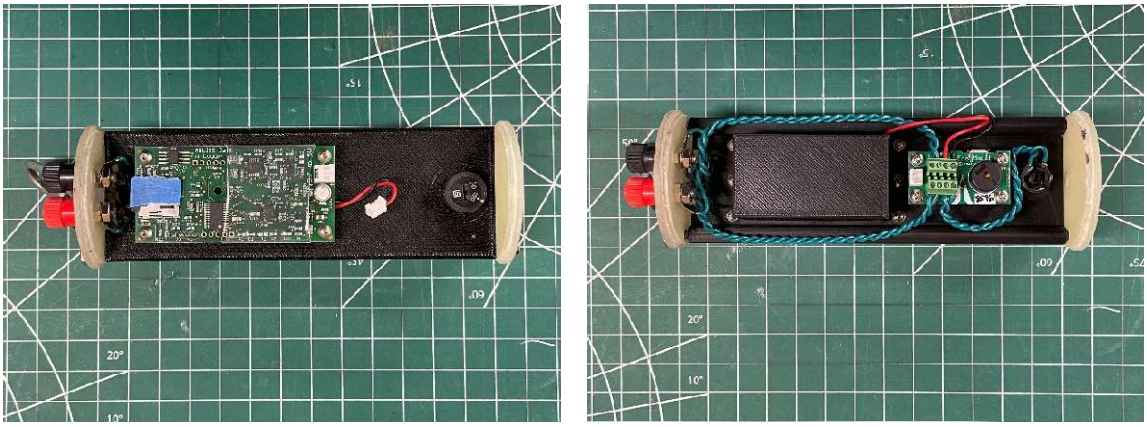

Figure 3-3 TR-1 electronics bay with RAF Datalogger (left) and Altus Metrum EasyMini (left)

The rate gyroscope will see the same angular rotation about each of its axes no matter where it is located along the rocket's length. But the acceleration the accelerometer sees is impacted by its location along the length of the rocket. The accelerometer will measure the acceleration due to thrust, gravity, drag, and any side-to-side motion of the rocket. The side-to-side motion will be a combination of any side-to-side motion of the center of gravity of the rocket plus the side-to-side motion due to the rocket's rotation about its x or y-axes if the accelerometer is located some distance from the center of gravity rotation point. To measure just the side-to-side motion of the center of gravity, any acceleration component due to the rotational arc must be subtracted from the total acceleration. This is possible by using the rate gyroscope to determine the rocket's rotation, along with knowing the distance between center of gravity and the accelerometer's location. But there is always a potential source of error in making the measurements for the correction, so it is better to minimize the rotational motion by placing the accelerometer as close as possible to the center of gravity to eliminate rotational arc acceleration component. In TR-1, the

[20] See Appendix 4 - Mapping Between 3-Dimensional Coordinate Systems

accelerometer is close enough to the center of gravity that the rotational component of the lateral acceleration can be neglected.

3.2 TR-1 Flight Data

The flight of TR-1 that will be analyzed in detail below occurred on October 15, 2022, at Tripoli Central's October Skies launch at the Maddox Dairy in Helm, California.

Figure 3-4 October 15, 2022, flight of TR-1 at October Skies

The flight data consists of the Altus Metrum barometric altitude data and the RAF Datalogger accelerometer and rate gyroscope data.

Figure 3-5 shows the altitude profile for the flight from the Altus Metrum altimeter data. The winds were relatively calm at 5 mph with gusts to 10 mph at ground level, and the rocket went nearly vertically, although the slight turn into the wind was noticeable as the rocket left the launch rail. Apogee was 1,606 feet at 9.38 seconds.

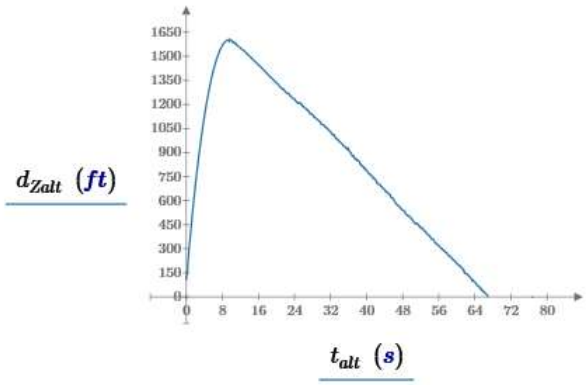

Figure 3-5 Altus Metrum barometric altitude profile

Figure 3-6 shows the raw rotational rate and acceleration data from the RAF Datalogger. The following analyses are all based on this data.

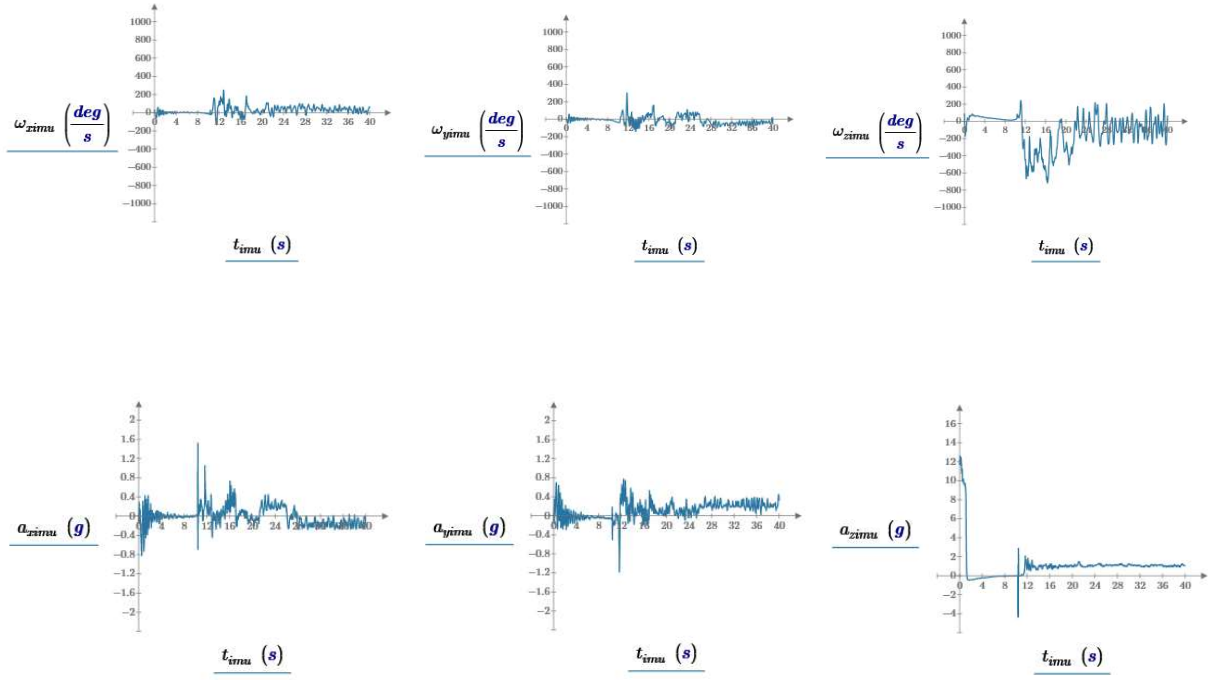

Figure 3-6 Raw rotational rate and acceleration data for the rocket's x, y, and z-axes

Euler's angles allow for mapping parameters between the rocket x-y-z frame of reference and the ground X-Y-Z inertial frame of reference. They are calculated from the x-y-z rotation rate data using equations (7.1-5) and are shown in Figure 3-7.

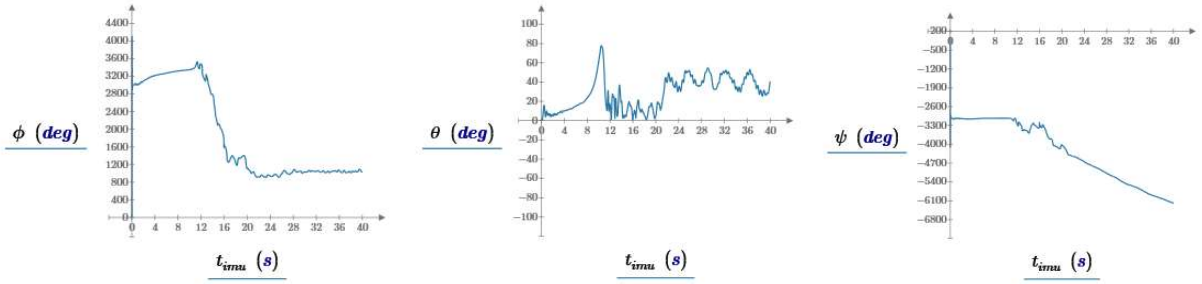

Figure 3-7 Euler's angles calculated form the rate gyroscope data

To find the acceleration of the rocket along its z-axis, the raw z-axis acceleration data must be corrected for the constant 1 g field due to gravity. Gravity is aligned with the ground frame-of-reference Z-axis, so the z component of the Z-axis unit vector is the portion of 1 g to subtract from the z-axis acceleration measured data. The Z-axis unit vector, shown in Figure 3-8, is calculated from (3.2-1) and Euler's angles equation. The notation U_{Zz} means the component of the Z-axis unit vector aligned in the direction of the z-axis. The z-axis of the rocket starts out aligned with the ground frame Z-axis but moves away from alignment as the rocket tilts into the wind. The rocket continues to rotate as it approaches apogee. The parachute deploys from the front end of the rocket which orients the accelerometer in the same direction it was oriented during the upward portion of the flight. 20 seconds into the flight, the rocket starts swinging under the parachute at a slight angle from vertical.

$$U_{Zz} = z_{Euler}(0,0,1) = \cos\theta \tag{3.2-1}$$

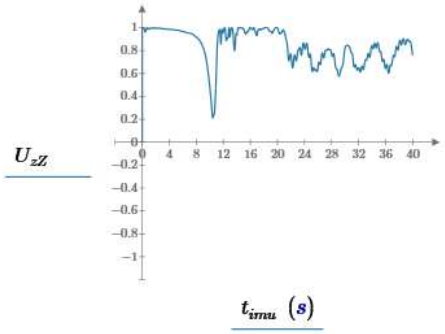

Figure 3-8 z component of the Z-axis unit vector

The gravitationally corrected z-axis acceleration and velocity are calculated by

$$a_{zcimu} = a_{zimu} - g \cdot U_{Zz} \tag{3.2-2}$$

$$v_{zcimu} = v_{zcimu} + a_{zcimu} \cdot \Delta t_{imu} \tag{3.2-3}$$

and shown in Figure 3-9. Once corrected for the gravitational field, the graph shows the acceleration ranged from 11.5 g's to 8.5 g's during thrust, then the rocket deaccelerated at a little more than -1 g due to a combination of gravity and drag during coast, approaching -1 g as the rocket slowed. Once the parachute deploys, the rocket has a constant velocity, so the acceleration stays at an average of 0 g's. At 20 seconds, the acceleration starts to show a net positive value due to the rocket's swinging under the parachute, producing a slight centrifugal acceleration. During recovery, the Datalogger faces forward, the same orientation as it is in flight, so the acceleration due to swinging is in a positive direction.

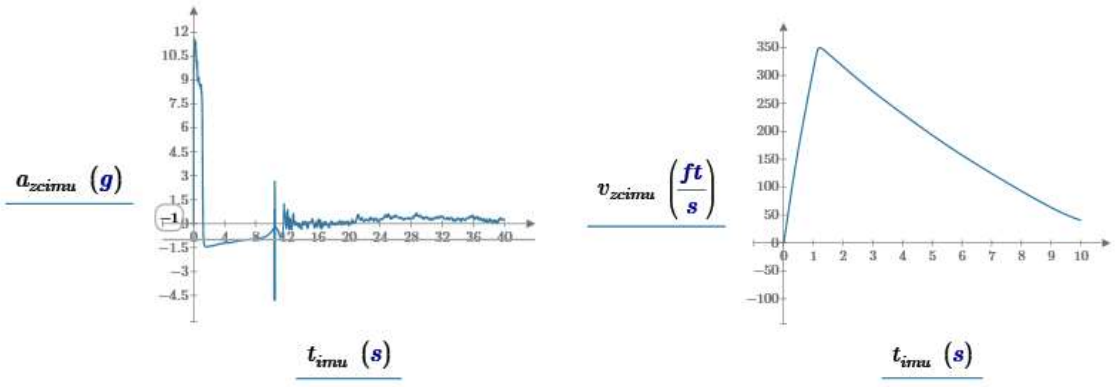

Figure 3-9 z-axis acceleration and velocity corrected for 1 g gravitational field

The polar angles are calculated from the z-axis unit vectors, equations (7.1-6), and shown in Figure 3-10. Θ, the polar angle from vertical, is the three-dimensional proxy for α_y, the orientation angle of the rocket from vertical in the 2-dimensional model. For this flight, the rocket rotated approximately 8 degrees as it left the launch rail, with a large initial overshoot in the step response, and the step response oscillations dampened over the next several seconds. The oscillation frequency starts around 3 Hz and slows as the rocket slows. Γ, the polar projection of the rocket's z-axis onto the XY plane, shows the rotation of the rocket's flight path projected onto the ground is constant at around 105 degrees. This indicates that the rocket flew in a 2-dimensional plane.

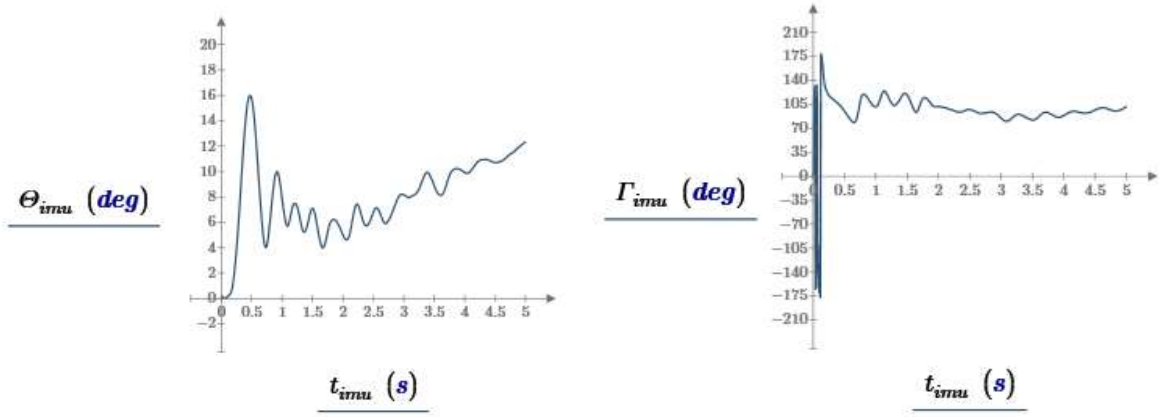

Figure 3-10 Polar angle s for the z-axis of the rocket in the ground (X-Y-Z) frame of reference

Figure 3-11 shows the spin rate and total angle of rotation about the rocket's z-axis. This shows that over the entire 10 seconds of the upward fight, the rocket rotates just one revolution. With minimal z-axis spin and the rocket's flight path falling along a two-dimensional plane, the two-dimensional model is valid for this fight.

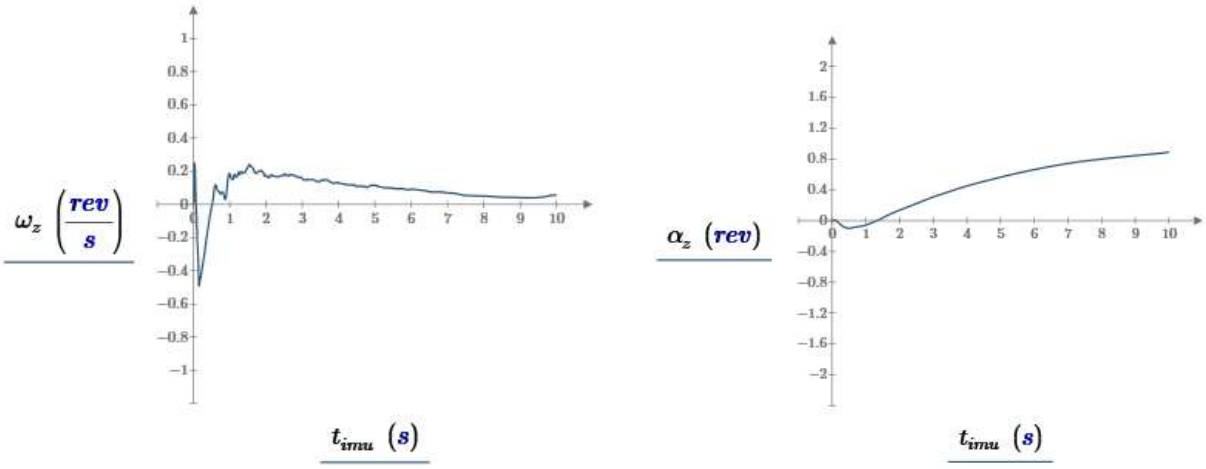

Figure 3-11 z-axis spin rate and rotational angle

The location of the tip of the nose cone in the ground-based frame of reference shows the rocket's attitude, and is given by the z- axis unit vector from equations (7.1-6). Plotting U_{zY} vs. U_{zX} in Figure 3-12 shows the trajectory of the tip of the nose cone in three dimensions projected onto the XY plane and viewed from above. On this graph, negative Y, north, is up and negative X, east, is to the right. After the initial turn into the wind toward the southeast, the rocket tip travels several times in a tight circle before starting to arc over at the end of the coast phase.

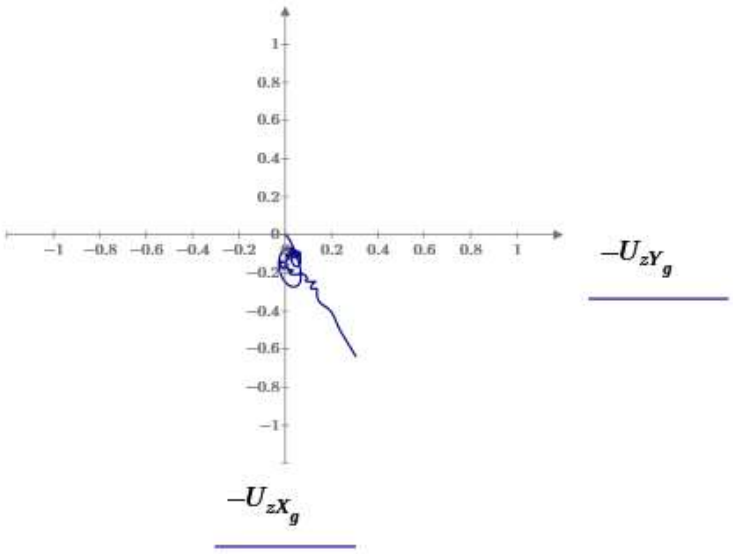

Figure 3-12 The projection of the motion of the tip of the nose cone onto the XY plane

The measurement of the flight path angle can be determined from the three-dimensional position data provided by the GPS. First, the GPS coordinate angles must be converted into linear feet along the lines of constant latitude and longitude on the surface of the earth. For the small changes in distance compared to the radius of the earth, it can be assumed that these changes map directly to a change in distance on the flat XY ground plane where latitude maps into the distance d_X along the X-axis and longitude maps into distance d_Y along the Y-axis. The equations to convert to latitude and longitude angel to feet are[21]

$$l_{latitude} = 365222.0 \cdot \alpha_{latitude} \tag{3.2-4}$$

$$l_{longitude} = 36217.6 \cdot \alpha_{longitude} \cdot \cos\left(\alpha_{latitude} \cdot \frac{2 \cdot \pi}{360}\right) \tag{3.2-5}$$

where the angle is in units of degrees distances are in feet.

[21] (Fetter T. B., 2015)

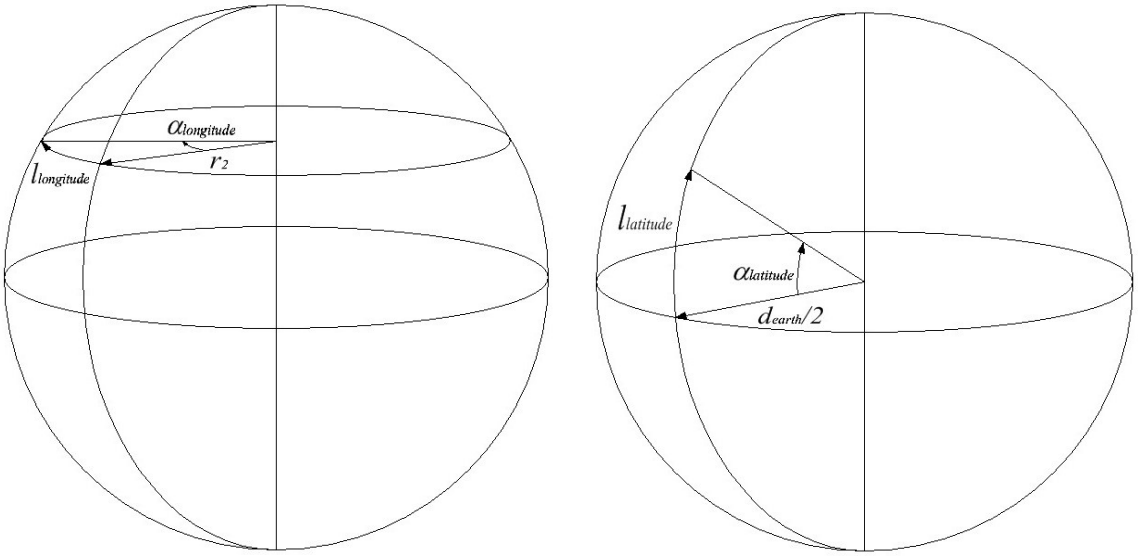

Figure 3-13 Distance along lines of constant longitude and latitude

The flight path angle from Figure 2-7 can then be calculated by

$$\theta_{CGgps_i} = \frac{\Delta_{XY}}{\Delta_Z} = \frac{\sqrt{(d_{X_i} - d_{X_{i-1}})^2 + (d_{Y_i} - d_{Y_{i-1}})^2}}{d_{Z_i} - d_{Z_{i-1}}} \tag{3.2-6}$$

3.3 Comparing the Model to Flight Data

To validate the 2-D flight model's prediction of the rocket's rotation due to the wind, the rotation rate flight data from the RAF Datalogger described in Sections 3.1 and 3.2 was used. Figure 3-14 shows the results of three flights of test rocket TR-1. For each, the left hand graph shows the modeled and measured rotational angle. For the measured angle, the 3-D polar angle is used as described in Section 3.2. For all three flights, a 10 mph wind velocity, which is typical for the launch site, was used in the model. For each flight, the right hand graph shows the z-axis rotation rate of the rocket which comes directly from the gyro data.

For all three flights, the frequency of oscillation and damping ratio, the rate the oscillations decrease, are a close match. The measured initial peak is a little larger than the simulation, but the oscillation quickly dampens to match the simulation. In the first two flights, the angle of rotation matches very closely, at around 7.5 deg.

For the third flight, the measured rotation angle is around 20 deg. From Figure 2-21, it would require a 26 mph velocity wind during the first several seconds of the launch to cause a 20 deg rotation, which is possible. Another possible cause of the large rotation is launch-guide whip which can cause rockets to rotate as they leave the launch guide. But the rails used here are the 1010 aluminum launch rails which are very stiff, especially for a rocket as small and light as test rocket TR1, so it is unlikely significant launch guide whip occurred on these flights. A short duration off axis thrust could have caused the excessive rotation at launch. The motor thrust is also a force acting on the rocket that can have a rotational component if the thrust is slightly off-axis. Larger than predicted rotations have been measured on other flights as well. But because the rockets are not launched in a controlled wind environment, it is not certain whether these are caused by the initial step in wind velocity or by one of these other mechanisms. More data needs to be gathered to determine how often these larger than predicted occur.

For all three flights, the z-axis spin rate of the rocket is low during the first 5 seconds of the flight, the time during which the rocket is responding to the initial step in wind velocity. A low spin rate is one of the requirements for the 2-D model to be valid to describe the rocket's rotation into the wind.

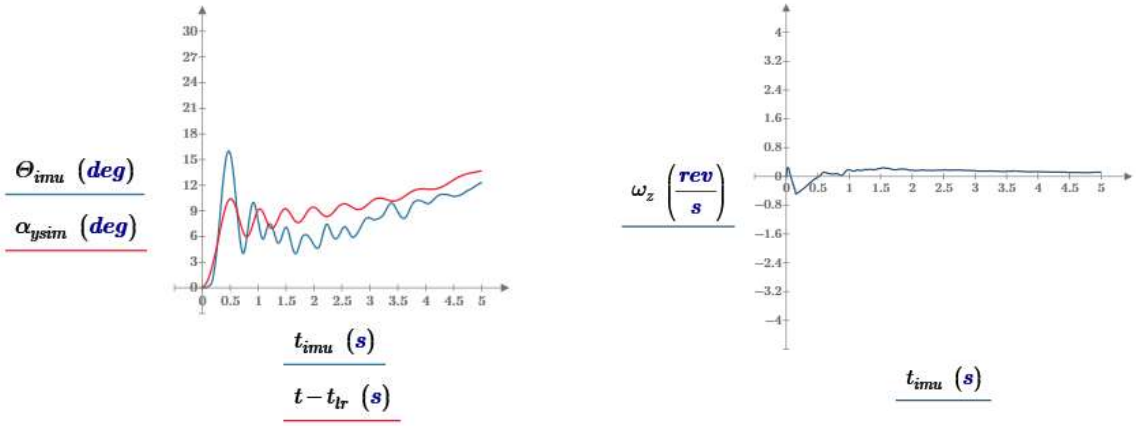

10/15/2022 flight

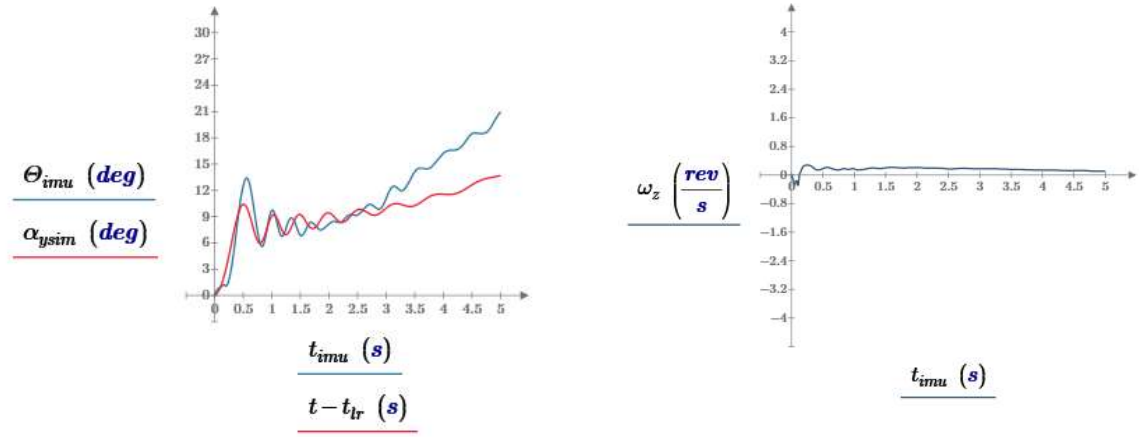

5/19/23 flight

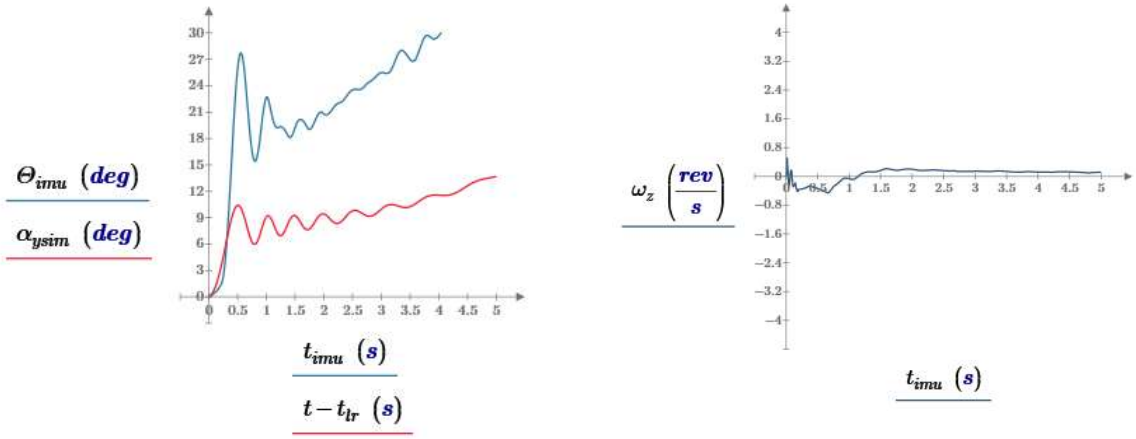

10/16/2022 flight

Figure 3-14 Three flights of TR-1 on an AT H128-W using a 10 mph wind step in simulation

The 5/19/23 flight of test rocket TR-1 included a Beeline GPS. Figure 3-15 shows the rotation and flight path angles including the measured flight path angle, θ_{gps} . The Beeline GPS only records one data point per second, so the first valid data point is one second into the flight. The measured flight angle parallels the modeled flight angle but is about 4 degrees greater. The flight angle determined from the GPS data is an absolute angle that includes the initial angle of the flight path due to the angle of the launch guide. The modeled for the flight path angles, θ_{CGsim} , assumes the launch angle is 0 deg. The GPS data shows that the angle of the launch guide was around 4 degrees. Had all the rotational angles included the initial tilt of the rocket, the flight path angles would match.

The 1 second data rate of the GPS data is not fast enough to capture the small oscillations in the flight path angle, but it does capture the long term trend. GPS units sometimes also s loose lock at launch due to the high acceleration, but in this case, lock was maintained.

The right hand graph in Figure 3-15 shows a projection of the GPS flight path onto the X-Y ground plane. The flight originates at 0,0, and flies along a straight line to the north-east, and then drifts to the south south-east under parachute. Because the upward portion of the flight occurs along a flat XY/Z plane, this also shows that the 2-D model is a valid representation of the rotational dynamics of the flight.

.

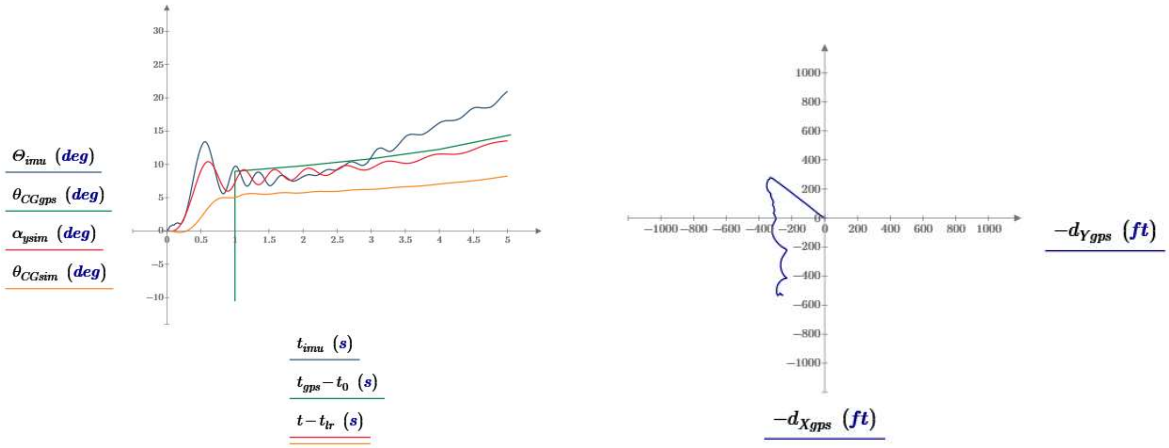

Figure 3-15 5/19/23 flight of TR-1 on an AT H128-W using a 10 mph wind step in simulation

4 Summary

- The two primary rotational angles are the rocket rotation angle of the rocket and the flight path angle
- The flight path angle is the rotation angle most easily observed from the ground as the angle that the rocket rotates into the wind
- The modeled rotational and flight angles were shown to generally agree with measurements from the flights of test rocket TR1
- If the wind step occurs before motor burnout, the rocket accelerates along the X-axis, increasing the flight path angle
- If the wind step occurs after motor burnout, the rocket rotates but does not accelerate along the X-axis and the flight path angle does not change due to the step in wind velocity
- The rocket's rotational angle is greater than the flight path angle because the rocket flies at an offset angle to its flight path angle determined by the ratio of the wind velocity to the forward velocity of the rocket
- The sensitivity studies show that there is not a direct correlation between the change in the stability margin (distance between the center of pressure and center of gravity) and the rocket rotation or flight path angles
- All the flight model parameters impact the rotation of the rocket into the wind, not just the distance between the center of pressure and the center of gravity (stability margin)
- Being over stable does not necessarily mean that the rocket will be more prone to rotating into the wind
- The increase in the total mass of the rocket that comes with an increase in the body tube length, fin size, nose weight mass, or material density, has a bigger impact on the maximum altitude of the rocket than does the increase in the magnitude of the rotational step response due to those parameters
- After changing a rocket design parameter (body tube length, fin size, nose weight mass), if the mass of the rocket is adjusted by changing the material density to bring it back to the mass of the rocket before the design parameter was changed, the rocket still turns nearly the same as the rocket without the adjusted density but reaches nearly the same maximum altitude as the original rocket
- In a wind, the rocket's maximum altitude is very sensitive to motor burn time
- There is an optimal burn time that optimizes altitude loss due to the rotation into the wind with altitude loss due to drag - the higher the wind, the shorter the optimal burn time
- To reach maximum altitude, minimizing the total mass is much more important than making changes that that just minimize the rocket's rotational or flight path angles.

5 Appendix 1 - Tools & Equipment

Mathcad was the main tool used on this project for modeling, numerical analysis, symbolic analyses, measurement data analysis, and graphing and analysis.

RockSim was used to validate the parameters calculated by the model such as moment of inertia and center of pressure.

Microsoft Office Word was used to write this paper

MathType embedded app for Office was used to create the equations in MS Word

TurboCAD was used to create most of the figures other than graphs and create the test rocket eBay sled design

PowerPoint was used to create some figures

The RAF Data Logger was used to measure the rocket's 3-D acceleration and axis rotations

A Beeline GPS was used to get flight path data and validate the wind speed at the flight time for comparing the model simulation to the measured rotational response

Test rocket TR-1 was built from standard off-the-shelf fiberglass parts from Mad Cow Rocketry.

A Dremel 3D45 3D printer was used to print the test rocket ebay sled

Numerous home shop woodworking shop tools were used to build the test rocket TR-1

All test flights were done at Tripoli Central's launch site at the Maddox Dairy in Helm California

6 Appendix 2 – 3-D Flight Model

This is the complete set of equations that is the starting point for a 3-dimensional flight trajectory and rotational dynamics model. The 2-dimensional model is a subset of this model.

Newton's law for the position of the CG in the inertial (ground) frame of reference

$$m_o \frac{d^2 d_X}{dt^2} = F_{TX} + F_{DX} + F_{LX} \tag{5.1-1}$$

$$m_o \frac{d^2 d_Y}{dt} = F_{TY} + F_{DY} + F_{LY} \tag{5.1-2}$$

$$m_o \frac{d^2 d_Z}{dt^2} = F_{TZ} + F_{DZ} + F_{LZ} - m_o g \tag{5.1-3}$$

Euler's dynamic equations for the rotation about the CG in the rocket frame of reference. This uses symmetry to eliminate the z-axis coupling with the x and y-axes ($\left(I_L - I_L\right) = 0$

$$I_L \frac{d^2 \alpha_x}{dt^2} = M_{2x} + M_{2Rx} + M_{1x} + (I_L - I_R) \cdot \frac{d\alpha_y}{dt} \cdot \frac{d\alpha_z}{dt} \tag{5.1-4}$$

$$I_L \frac{d^2 \alpha_y}{dt^2} = M_{2y} + M_{2Ry} + M_{1y} + (I_R - I_L) \cdot \frac{d\alpha_x}{dt} \cdot \frac{d\alpha_z}{dt} \tag{5.1-5}$$

$$I_R \frac{d^2 \alpha_z}{dt^2} = M_{2z} + M_{1z} \tag{5.1-6}$$

Euler's angles for translation from the rocket frame of reference to the inertial (ground) frame of reference. These rotation rate equations are consistent with the conventions used in Sidi[22] but the derivation is shown in Thomson[23] using a different order of rotation convention

$$\frac{d\phi}{dt} = \omega_x + \frac{\sin\theta \sin\phi}{\cos\theta} \cdot \omega_y + \frac{\cos\phi \sin\theta}{\cos\theta} \cdot \omega_z \tag{5.1-7}$$

$$\frac{d\theta}{dt} = \cos\phi \cdot \omega_y - \sin\phi \cdot \omega_z \tag{5.1-8}$$

[22] (Sidi, 2002, p. Appendix A)

[23] (Thomson, 1986, p. 38)

$$\frac{d\psi}{dt} = \frac{\sin\phi}{\cos\theta} \cdot \omega_y + \frac{\cos\phi}{\cos\theta} \cdot \omega_z \tag{5.1-9}$$

7 Appendix 3 – 2-D Flight Model

Figure 7-1 shows the 2-dimensional, 3 degree-of-freedom model. X and Z are used to denote the fixed ground frame axes, rather than X and Y, to be consistent with the conventions that are used in the 6 degree-of-freedom model where Z is the vertical axis. In this system, the Y-axis is coming out of the plane of the figure. An angle of rotation is denoted by the axis about which the object rotates. Since the rocket frame of reference axes, x, y, and z, start out aligned with the ground-based frame of reference axes, X, Y, and Z, in the three-dimensional model, the rocket, in the two-dimensional model, rotates about its y-axis. In the two-dimensional model, the rocket's y-axis always remains orthogonal to the plane of the ground XZ-axes and aligned with the Y-axis. To be consistent with the 6 degree-of-freedom model, the y-axis will be used as the axis of rotation of the rocket, even though the y-axis is not shown explicitly in the 2-dimensional drawings. The direction of rotation about the y-axis shown in Figure 7-1 indicates the positive direction for a right-handed coordinate system where the positive y-axis comes out of the drawing.

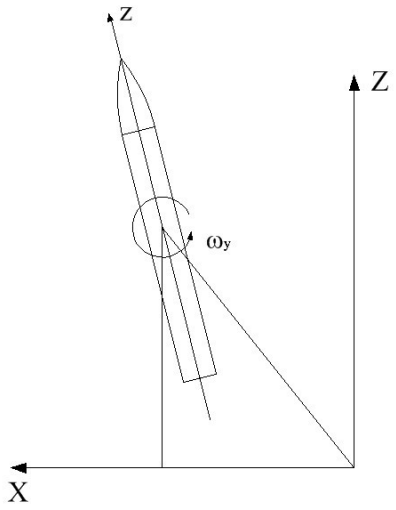

Figure 7-1 Model for 3-degrees of freedom

There are three second order differential equations of motion that must be solved simultaneously to determine the trajectory and orientation of a rocket in flight in the 2-dimensional model. The first two equations describe the motion of the center of gravity of the rocket along the X and Z-axes in the ground-based frame of reference and the last one describes the rotation about the y-axis in the rocket frame of reference. In the 2-dimensional system, the translation from the rocket frame of reference to the inertial ground frame of reference is just the rotational angle of the rocket, α_y, so no additional axis translation equations are required.

$$m_o \frac{d^2 d_X}{dt^2} = F_{TX} + F_{DX} + F_{LX} \tag{6.1-1}$$

$$m_o \frac{d^2 d_Z}{dt^2} = F_{TZ} + F_{DZ} + F_{LZ} - m_o g \tag{6.1-2}$$

$$I_L \frac{d^2 \alpha_y}{dt^2} = M_{2y} + M_{2R} + M_{1y} \tag{6.1-3}$$

Each second order differential equation can be written in terms of two first order differential equations. This is the convention used by a state variable system which defines the state variables in terms of first order differential equations. The state variable convention is used here to be consistent with the form used by Mathcad for solving nonlinear simultaneous differential equations numerically.

$$\frac{dd_X}{dt} = v_X \tag{6.1-4}$$

$$m_o \frac{dv_X}{dt} = F_{TX} + F_{DX} + F_{LX} \tag{6.1-5}$$

$$\frac{dd_Z}{dt} = v_Z \tag{6.1-6}$$

$$m_o \frac{dv_Z}{dt} = F_{TZ} + F_{DZ} + F_{LZ} - m_o g \tag{6.1-7}$$

$$\frac{d\alpha_y}{dt} = \omega_y \tag{6.1-8}$$

$$I_L \frac{d\omega_y}{dt} = M_{2y} + M_{2R} + M_{1y} \tag{6.1-9}$$

These six differential equations will be used to solve for the six state variables as a function of time. The six variables are $d_X, v_X, d_Z, v_Z, \alpha_y,$ and ω_y. They describe the rocket's location and rotational angle in 2-dimensional space, as well as its velocity and rate of angular rotation. These six variables are referred to as the state variables of the system because they are the minimum number of variables needed to completely describe the state of the system at any instant in time. Once the state variables are determined, all other parameters of interest can be found from the state variables using algebraic equations that are functions of the state variables. All parameters in the model are written as functions of these six variables, plus the two inputs to the model, the motor thrust and the wind velocity.

Because the state variables are all functions of time or frequency, it is common, to use the nomenclature $\alpha_y(t)$ in the time domain equations, and $\alpha_y(s)$ in the frequency domain equations when writing the state variable α_y. This paper will simply use the nomenclature α_y to keep the equations simpler and easier to read, and the context of the equation to determine whether the variable is a time or frequency domain variable.

The key velocity vectors and angles used by the model are shown in Figure 7-2. Figure 7-3 shows the velocity relationships in more detail. The model assumes that the wind that causes the rocket to rotate is approaching from the -X (westerly) direction. The rocket rotates into the upper left-hand quadrant as a result. v_T is the velocity of the total oncoming airstream.

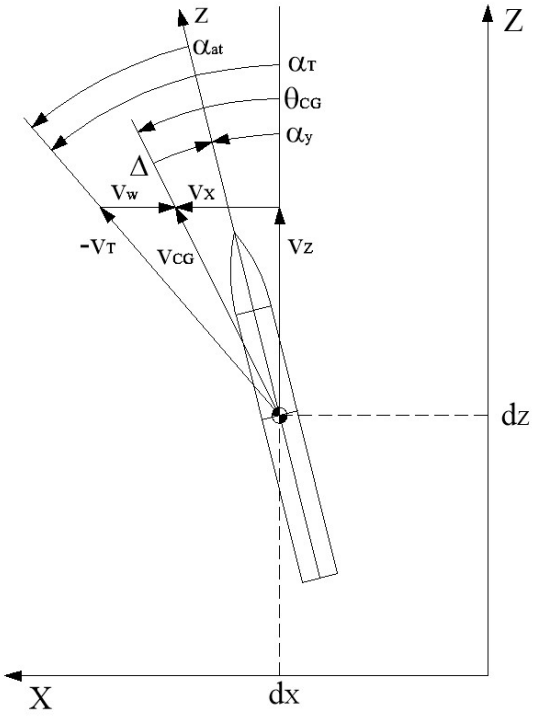

Figure 7-2 Key rotational angles

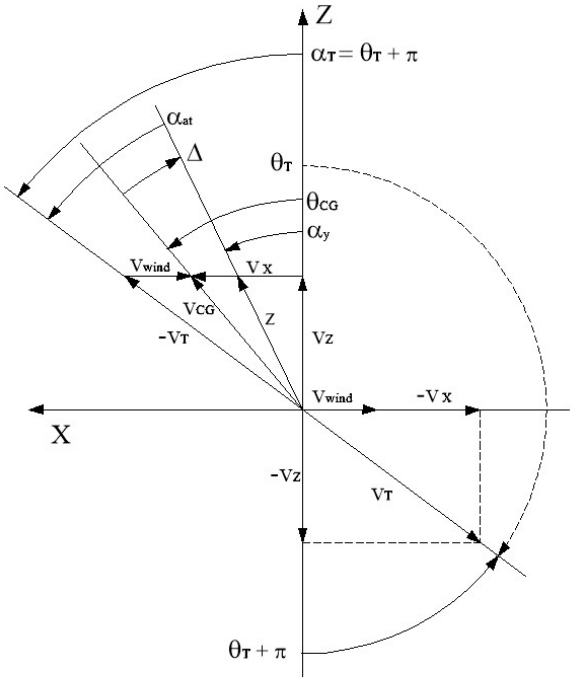

Figure 7-3 Key velocity vectors and angles

Rather than stating equations (6.1-4) to (6.1-9) directly in terms of the state variables, which makes the equations very long, intermediate functions are used. The intermediate variables also provide insight into the behavior of the model. The following equations define the intermediate variables in terms of the state variables of the system.

θ_{CG} is the angle of the velocity vector, v_{CG} , of the center of gravity of the rocket, which is not necessarily the same direction as the rocket is pointed. It is defined by the X and Z-axis velocities.

$$\theta_{CG} = \arctan\frac{v_X}{v_Z} \tag{6.1-10}$$

Δ is the difference between the direction the rocket traveling and the rocket is pointed

$$\Delta = \theta_{CG} - \alpha_y \tag{6.1-11}$$

The Z-axis component of the oncoming airstream is the negative of the Z component of the rocket's velocity. The X -axis component of the oncoming airstream is the negative of the X-axis component of the rocket's velocity plus the velocity of the wind. The total oncoming airstream velocities are

$$v_{TX} = v_w - v_X \tag{6.1-12}$$

$$v_{TZ} = -v_Z \tag{6.1-13}$$

$$v_T = \sqrt{{v_{TX}}^2 + {v_{TZ}}^2} = \sqrt{(v_w - v_X)^2 + {v_Z}^2} \tag{6.1-14}$$

θ_T is the angle of the total oncoming airstream. Since the airstream is opposite the direction of the rocket's velocity, the angle is in the quadrant opposite the rocket's direction of travel. α_T is the angle of the oncoming airstream reflected back into the quadrant of the rocket's travel.

$$\theta_T = -\arcsin\frac{v_{TX}}{v_T} + \pi = -\arcsin\frac{v_w - v_X}{v_T} + \pi \tag{6.1-15}$$

$$\alpha_T = \theta_T - \pi = -\arcsin\frac{v_w - v_X}{v_T} \tag{6.1-16}$$

The angle of attack is the difference between the angle of the negative of the oncoming airstream and the rotation angle of the rocket's rotation

$$\alpha_{at} = \alpha_T - \alpha_y \tag{6.1-17}$$

The trajectory force equations are[24]

$$F_{DX} = \frac{\rho}{2} \cdot A_r \cdot C_D \cdot {v_T}^2 \cdot \sin\theta_T \tag{6.1-18}$$

$$F_{DZ} = \frac{\rho}{2} \cdot A_r \cdot C_D \cdot {v_T}^2 \cdot \cos\theta_T \tag{6.1-19}$$

$$F_{LX} = \frac{\rho}{2} \cdot A_r \cdot C_{L\alpha} \cdot \alpha_{at} \cdot {v_T}^2 \cdot \cos\theta_T \tag{6.1-20}$$

$$F_{LZ} = -\frac{\rho}{2} \cdot A_r \cdot C_{L\alpha} \cdot \alpha_{at} \cdot {v_T}^2 \cdot \sin\theta_T \tag{6.1-21}$$

[24] (Mandell, Caporaso, & Bengen, 1973)

$$F_{TX} = F_T \cdot \sin \alpha_y \tag{6.1-22}$$

$$F_{TZ} = F_T \cdot \cos \alpha_y \tag{6.1-23}$$

and the rotational force and moment equations are

$$F_{N1y} = -\frac{\rho}{2} \cdot A_r \cdot C_{N\alpha} \cdot v_T{}^2 \cdot \alpha_{at} \tag{6.1-24}$$

$$F_{N2y} = +\frac{\rho}{2} \cdot A_r \cdot C_{N\alpha} \cdot v_T \cdot \omega_y \cdot (L_{CP} - L_{CG}) \tag{6.1-25}$$

$$M_{1y} = -F_{N1y} \cdot (L_{CP} - L_{CG}) \tag{6.1-26}$$

$$M_{2y} = -F_{N2y} \cdot (L_{CP} - L_{CG}) \tag{6.1-27}$$

$$M_{2R} = -\frac{L_m \cdot m_p}{6 \cdot t_b} \cdot (3 \cdot L_{ne} - 3 \cdot L_{CG} - L_m) \cdot \omega_y \tag{6.1-28}$$

Equations (6.1-4) to (6.1-28) are the complete model of a rocket in flight needed to describe its location and orientation in 2-dimensional space. The 6 first order differential equations (6.1-4) to (6.1-9) that solve for the 6 state variables are nonlinear, so they cannot be solved in closed form, but they can be solved numerically using the rkfixed function in Mathcad[25].

For small angles of attack, the lift coefficient, $C_{L\alpha}$, is assumed to be the same as the normal force coefficient, $C_{N\alpha}$. The value of the normal force coefficient is determined using the methods described by Barrowman[26]. The drag coefficient is determined from RockSim[27].

Figure 7-4 shows examples of the output of the complete Mathcad flight model using the parameters for the test rocket TR-1. The physical parameters for TR-1 are given in Section 3.1. Most of the graphs in this paper are based on the output of the model using the TR-1 parameters.

---

[25] (Mathcad Home Page, n.d.)

[26] (Barrowman J. , 1968)

[27] (RockSim, 2024)

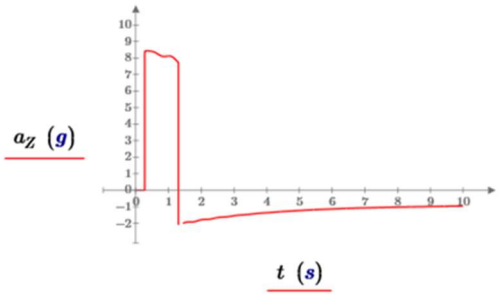

Z-axis acceleration

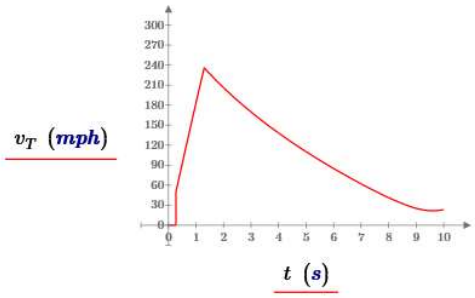

Total incident airstream velocity

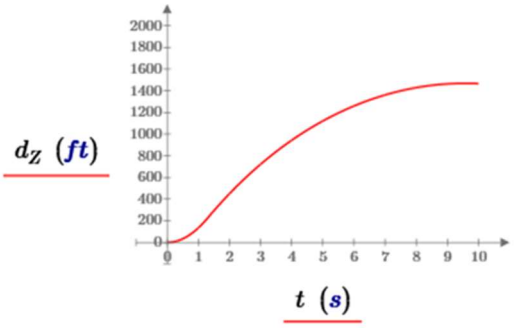

Z-axis distance (altitude)

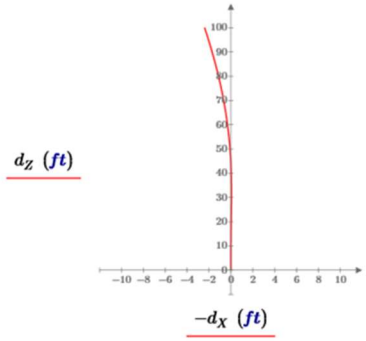

Trajectory

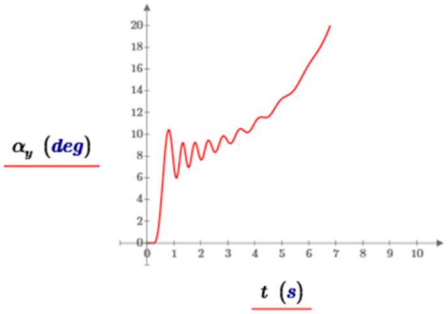

Rotation angle of the rocket

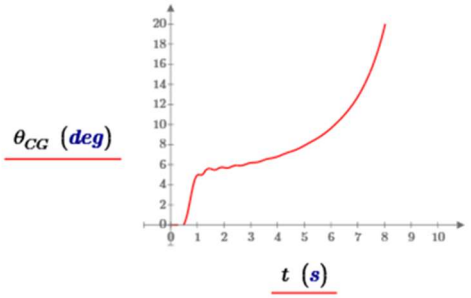

Flight path trajectory angle

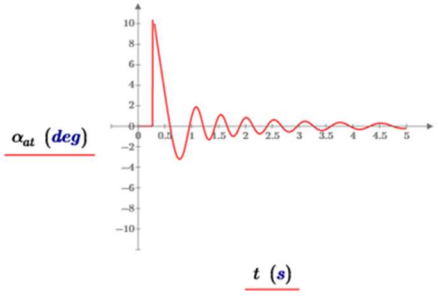

Angle of attack

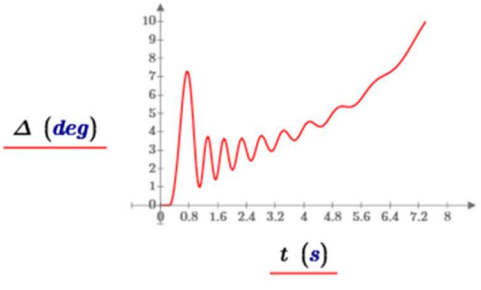

Difference between the rocket rotation angle and the flight path angle

Figure 7-4 Example of the output of the complete trajectory and rotational stability model using the parameters for test rocket TR-1 flying on an AT H128W motor and a 10 mph step in wind velocity as the rocket leaves the launch guide

Figure 7-5 shows a comparison between the flight model (red trace) and flight data (blue trace) from test rocket TR-1. The altitude prediction matches very closely, and the rotation angles match very closely over the first three seconds assuming an initial 10 mph step in wind velocity.

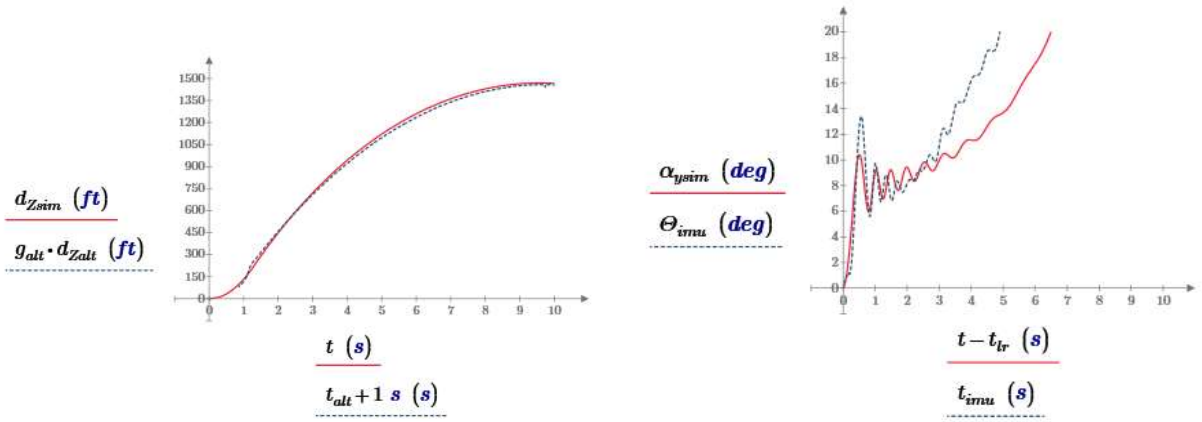

Figure 7-5 Comparing the model to flight data from 5/19/23 flight of TR-1 assuming a 10 mph wind

Figure 7-6 shows a comparison of the forcing moment, the top graph, the rotational rate damping moment, the left graph, and the jet damping moment, the right graph for TR-1. The jet damping aligns in phase with the rotational rate damping, so it adds to the overall damping of the system, as expected. For the AT-H128W motor used in test rocket TR-1, the magnitude of the jet damping calculated using the core burning motor equation is less than one tenth the rotational damping magnitude, so the jet damping would add very little to the rocket's rotational stability. The core burner model was used for all the simulation results presented in this paper as it matches the geometry of the motor used. Also note that the jet damping only contributes for the length of the motor burn.

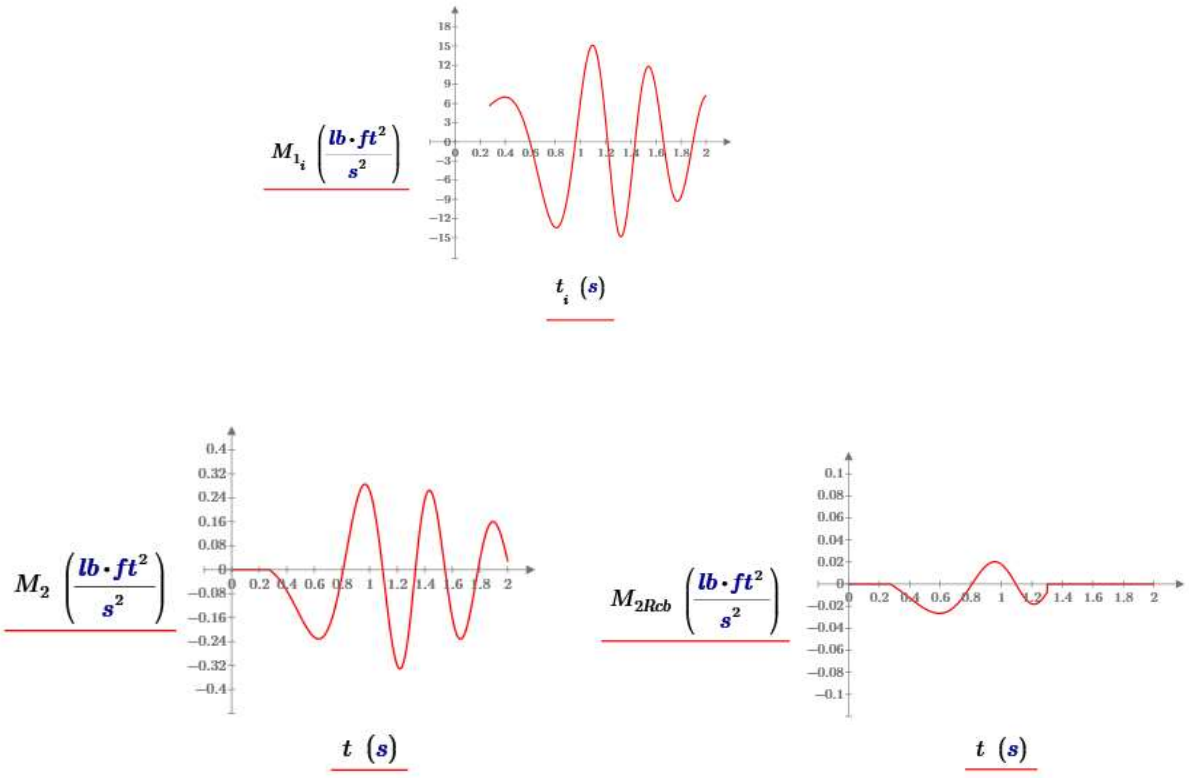

Figure 7-6 Comparing the forcing moment, M_1, rotational rate damping moment, M_2, and the jet damping moment calculated for a core burning motor, M_{2Rcb}, for test rocket TR-1 flying on an AT H128W motor and a 10 mph step in wind velocity

8 Appendix 4 - Mapping Between 3-Dimensional Coordinate Systems

Although the dynamic stability model presented here is a 2-dimensional model, the rocket that is used to collect data to verify the model flies in 3-dimensional space. If the rocket has minimal z-axis spin and the rocket flies in a single plane, the 2-D model is an accurate model of its dynamic behavior. But to be accurate, even with minimal spin, the motion of the actual rocket flight must first be determined in 3-dimensions and then mapped to 2-dimensions.

In the 2-D system, the rocket can only rotate only about a single axis. A rotation through a single angle is all that is required to map the rocket axis into the ground frame axis system. In the 3-D system, the mapping from then x-y-z rocket axis system to the ground-based X-Y-Z system, is not as simple. As shown in Figure 8-1, the rocket can rotate about all three axes in the rocket frame of reference, and since the x-y-z axis system follows the rocket, the x-y-z axes can be in any orientation in the ground X-Y-Z coordinate system. There are several methods for determining the location of a coordinate point in one axis system in the other rotated coordinate system. Quaternions, one method, does the translation in a single rotation step. Euler's angles does the translation in three orthogonal rotations through two intermediate axis systems. Quaternions have advantages, including computational efficiency and a lack of singularities. Euler's angles, used here, are easier to understand and work fine for post-processing flight data.

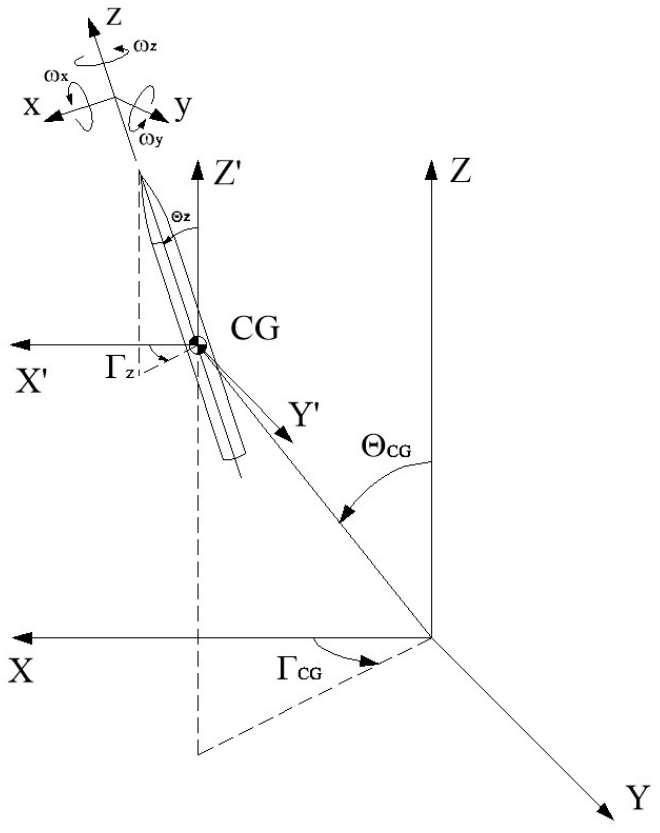

Figure 8-1 Orientation of the rocket in 3-dimensional space

Using Euler's angles, it takes three separate rotations to map between two 3-dimensional coordinate systems at arbitrary orientations relative to each other. Each rotation is described by an angle, so it takes three rotation angles to describe the orientation of one axis system relative to the other. Those rotation angles are called the Euler's angles and are denoted ϕ, θ, and ψ. The equations that are used to map between two coordinate systems are called Euler's angle equations.

Rotating an object about its x, y, and z-axes will result in a different final orientation depending upon the order in which the rotations are done. For a given rotation angle about each axis, the order sequence, x-y-z, y-x-z, or z-x-y, will result in different final locations for each sequence. The same order of rotation must be used to end up in the same final orientation each time a sequence is done. Therefore, the equations that are used to map between 3-D coordinate systems are unique to the order of each of the intermediate axis rotations used to derive the angle equations. A different order will result in a different set of Euler's equations and angles. For Euler's angles to work, the same rotational order used to derive the Euler's angles equations must then be used to translate between the two axis systems using those angles.

Three sets of three equations are needed when using Euler's angles. The first two sets of equations are used to translate a coordinate point between two rotated coordinate systems using Euler's angles. The third set of equations is used to find Euler's rotation angles for the current orientation of the two axes systems. The order convention means that all three sets of equations must have been derived using the same order of rotation convention.

There are numerous sources that cover the derivation of Euler's angles[28] that offer good explanations of the derivation. The equations used here are based upon the order of rotation conventions used in *Spacecraft Dynamics & Control*[29] in the order of rotation: ϕ about x, θ about y, and ψ about z.

Euler's equations translate the coordinates of a point in one axis system into the coordinates of that point in a second axis system, where the two axis systems can be at any spatial orientation relative to each other, as described by Euler's angles. This first set of Euler's equations map a point, (x, y, z) in the rocket frame, into a point (X, Y, Z) in the ground frame.

---

[28] Two examples are (Thomson, 1986, p. Chapter 3) and (Sidi, 2002, p. Appendix A)

[29] (Sidi, 2002, p. 321)

$$X_{Euler}(x,y,z) = (\cos\theta\cos\psi)\cdot x + (\cos\psi\sin\theta\sin\phi - \cos\phi\sin\psi)\cdot y + (\sin\psi\sin\phi + \cos\psi\cos\phi\sin\theta)\cdot z$$

$$Y_{Euler}(x,y,z) = (\cos\theta\sin\psi)\cdot x + (\sin\theta\sin\psi\sin\phi + \cos\psi\cos\phi)\cdot y + (\cos\phi\sin\theta\sin\psi - \cos\psi\sin\phi)\cdot z \quad (7.1\text{-}1)$$

$$Z_{Euler}(x,y,z) = (-\sin\theta)\cdot x + (\cos\theta\sin\phi)\cdot y + (\cos\theta\cos\phi)\cdot z$$

Conversely, a point in the ground frame can be mapped to the rocket frame by the second set of Euler's equations.

$$x_{Euler}(X,Y,Z) = (\cos\theta\cos\psi)\cdot X + (\cos\theta\sin\psi)\cdot Y - (\sin\theta)\cdot Z$$

$$y_{Euler}(X,Y,Z) = (\cos\psi\sin\theta\cdot\sin\phi - \cos\phi\sin\psi)\cdot X + (\sin\theta\sin\psi\sin\phi + \cos\psi\cos\phi)\cdot Y + (\cos\theta\sin\phi)\cdot Z$$

$$z_{Euler}(X,Y,Z) = (\sin\psi\sin\phi + \cos\psi\cos\phi\sin\theta)\cdot X + (\cos\phi\sin\theta\sin\psi - \cos\psi\sin\phi)\cdot Y + (\cos\theta\cos\phi)\cdot Z \quad (7.1\text{-}2)$$

The equations above require knowing Euler's angles at any moment in time. As the rocket rotates about its axes, the axes follow it, so the rocket axes are rotating in the ground-based frame of reference, and the Euler's angles are changing continuously. The sensor that is used to determine the rate of rotation is a rate gyroscope. A rate gyroscope provides the rate of rotation, ω, about each of the rocket's three axes, *x*, *y*, and *z*.

The rotation rate version of Euler's angles[30] are used to find Euler's angles. They determine the change in Euler's angles in terms of the rate of rotation about each of the rocket's x, y, and z-axes, ω_x, ω_y, and ω_z, the output of the rate gyroscope. Based on the same order convention used above, the continuous time version of these equations is

$$\frac{d\phi}{dt} = \omega_x + \frac{\sin\theta\sin\phi}{\cos\theta}\cdot\omega_y + \frac{\cos\phi\sin\theta}{\cos\theta}\cdot\omega_z$$

$$\frac{d\theta}{dt} = \cos\phi\cdot\omega_y - \sin\phi\cdot\omega_z \quad (7.1\text{-}3)$$

$$\frac{d\psi}{dt} = \frac{\sin\phi}{\cos\theta}\cdot\omega_y + \frac{\cos\phi}{\cos\theta}\cdot\omega_z$$

[30] These rotation rate equations are consistent with the conventions used above, but the derivation is shown in (Thomson, 1986, p. 38) using a different order of rotation convention

The rate equations give the continuous rate of change of Euler's angles for continuous rotation rates about each of the x, y, and z axes. If the rate of rotation about each of the axes is measured continuously from a known starting orientation, then the absolute orientation of the rocket axis system can be determined at any instant in time. Because the rotation about each of the three axes is being measured continuously, the order of rotation no longer matters, as the angular change about each of the axes in any instant of time approaches zero.

To find Euler's angles at any point in time, t_1, the rate equation is integrated, or summed continuously, from the starting point to that point in time

$$\psi(t_1) = \int_0^{t_1} \frac{d\psi(t)}{dt} dt \tag{7.1-4}$$

The rate gyro measures the rotation rate at a fixed sample rate, for example, 100 samples per second. If the sample rate is fast compared to the rate of rotation, it effectively looks like a continuous time measurement, that is, the sample rate must be much greater than the bandwidth of the rocket's rotational dynamics.

The data is handled as a discrete time system, so the continuous time differential equations become discrete time difference equations. To solve for Euler's angles from the change in Euler's angles, a discrete time integration is used where

$$\frac{d\psi}{dt} \rightarrow \frac{\Delta\psi}{\Delta t}$$

and

$$\Delta t = t_{samp} = t_n - t_{n-1}$$

And the integration is a continuous running sum

$$\psi = \psi + \Delta\psi \cdot t_{samp}$$

$$\phi = \Delta\phi + \phi \cdot t_{samp}$$

$$\theta = \theta + \Delta\theta \cdot t_{samp}$$

which leads to the solution for Euler's angles at each data point, *n*

$$\psi_n = \psi_{n-1} + \left[\frac{\sin\phi_{n-1}}{\sin\theta_{n-1}} \cdot \omega_{xn} + \frac{\cos\phi_{n-1}}{\sin\theta_{n-1}} \cdot \omega_{yn} \right] \cdot (t_n - t_{n-1})$$

$$\phi_n = \phi_{n-1} + \left[-\frac{\sin\phi_{n-1}\cos\theta_{n-1}}{\sin\theta_{n-1}} \cdot \omega_{xn} - \frac{\cos\phi_{n-1}\cos\theta_{n-1}}{\sin\theta_{n-1}} \cdot \omega_{yn} + \omega_{zn} \right] \cdot (t_n - t_{n-1}) \qquad (7.1\text{-}5)$$

$$\theta_n = \theta_{n-1} + \left[\cos\phi_{n-1} \cdot \omega_{xn} - \sin\phi_{n-1} \cdot \omega_{yn} + \omega_{zn} \right] \cdot (t_n - t_{n-1})$$

where $\psi_0 = 0$, $\phi_0 = 0$, and $\theta_0 = 0$. Once the value of Euler's angles are determined for each point in time as the rocket rotates about each of its axes, the location of any coordinate point in the rocket frame can be determined in the ground frame by using equations (7.1-1), and any coordinate point in the ground frame can be determined in the rocket frame by using equations (7.1-2).

The orientation of the rocket's z-axis in the X-Y-Z axis system can be used to determine the orientation of the rocket for an observer on the ground. Figure 8-2 shows an example of the path the tip of the nosecone takes during the rocket's flight. That point is determined by plotting the coordinate point (X,Y,Z) in the ground frame where (X,Y,Z) is determined by solving equations (7.1-1) for (x,y,z) = (0,0,1), or the unit vector of the z-axis of the rocket, U_z. For the z-axis unit vector, the equations (7.1-1) become

$$U_{zX} = X_{Euler}(0,0,1) = \sin\theta\sin\psi$$

$$U_{zY} = Y_{Euler}(0,0,1) = -\sin\theta\cos\psi \qquad (7.1\text{-}6)$$

$$U_{zZ} = Z_{Euler}(0,0,1) = \cos\theta$$

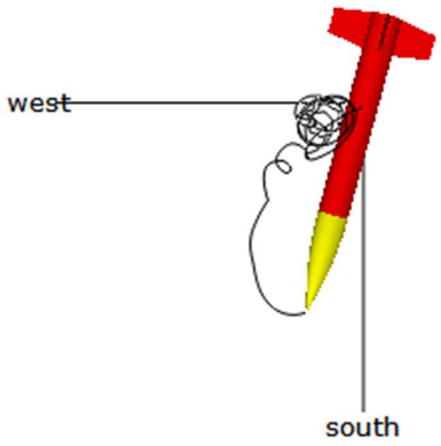

Figure 8-2 Visualization of the spherical path taken by the tip of the rockets nosecone during flight looking down toward the ground from above (SpeedRunner 75 5/21/2016)

The rotation of the rocket about its z-axis (spin) can be determined by either the x or the y-axis unit vector. Other quantities, such as distance, velocity, and acceleration, can also be translated between the frames of reference using Euler's angles.

Polar coordinates are used to describe the orientation of the rocket using the flight data. The 3-D angle of the rocket from vertical that is equivalent to the 2-D angle, α_y is calculated by finding the polar coordinates of the rocket's z-axis unit vector. Once the X, Y, and Z values are determine for the z-axis unit vector from equations (7.1-6), then its polar coordinates can be found.

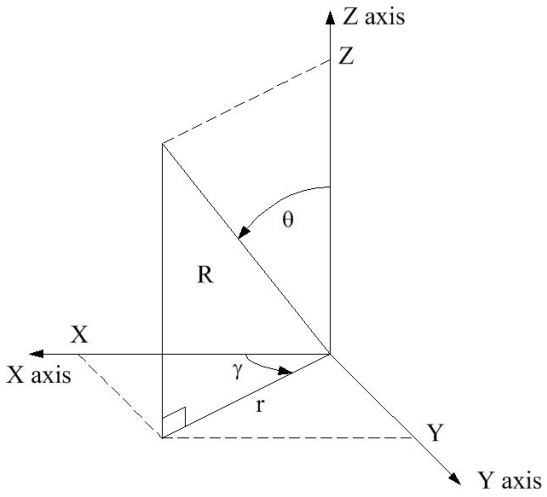

Figure 8-3 Spherical & Cartesian Coordinates

To go from Cartesian to spherical coordinates

$$r = \sqrt{X^2 + Y^2} \tag{7.1-7}$$

$$R = \sqrt{Z^2 + r^2} = \sqrt{X^2 + Y^2 + Z^2} \tag{7.1-8}$$

Then, the polar coordinates are

$$\Theta = \arcsin\frac{r}{R} = \arcsin\frac{\sqrt{X^2 + Y^2}}{\sqrt{X^2 + Y^2 + Z^2}} \tag{7.1-9}$$

$$\Gamma = \arcsin\frac{Y}{\sqrt{X^2 + Y^2}} \tag{7.1-10}$$

where Θ is the 3-D equivalent of the 2-D α_y.

9 Key Variables

A_r	cross-sectional area of the rocket
C_1	rotational forcing coefficient
C_2	rotational damping coefficient
C_3	X-axis forcing coefficient
C_4	rotational velocity damping coefficient
C_1'	coupled forcing coefficient
C_2'	coupled damping coefficient
C_D	drag coefficient
$C_{L\alpha}$	lift coefficient
$C_{N\alpha}$	normal force coefficient
CP	center of pressure
CG	center of gravity
d_X	distance traveled along the ground frame X axis
d_{Xss}	distance the rocket travels along the X-axis due to the small side-to-side motion
$d_{\alpha y}$	distance the rocket travels along the X-axis from the projection of the y-axis rotational velocity to the center of pressure
d_Z	distance traveled along the ground frame Z axis
F_D	the drag force – X and Y subscripts are used to denote the drag force along the X and Z axes
F_L	the lift force – X and Y subscripts are used to denote the lift force along the X and Z axes
F_N	the normal force
F_G	the force due to gravity
F_T	the thrust force – X and Y subscripts are used to denote the thrust force along the X and Z axes
g	acceleration due to gravity
$G_{\alpha y}$	rotational dynamics frequency domain gain function
$K_{\alpha y}$	dc gain of the linearized rotational dynamics frequency domain gain equation
K_{vX}	dc gain of the linearized X-axis frequency domain gain equation
I_L	longitudinal moment of inertia
L_{CP}	distance from the tip of the nosecone to the center of pressure

L_{CG} distance from the tip of the nosecone to the center of gravity

L_m length of the motor

L_{ne} length from the tip of the nosecone to the base of the rocket

m_o mass of the rocket

m_p mass of the propellant

M_R the total rotational moment about the center of the object – for the rocket, this would be the tip of the nosecone

M_{1y} rotational forcing moment

M_{2y} rotational damping moment

M_{2R} rotational jet damping moment

s complex frequency $s = j \cdot \omega$

t time

t_b burn time of the motor

U_{zX} the X-axis component of the z-axis unit vector in 3-dimensional space

U_{zY} the Y-axis component of the z-axis unit vector in 3-dimensional space

U_{Zz} the z-axis component of the Z-axis unit vector in 3-dimensional space

v_{CG} the velocity of the center of gravity of the rocket

v_T the velocity of the total oncoming airstream

v_w the velocity of the wind along the X-axis

v_X the velocity of the rocket along the X-axis

v_Z the velocity of the rocket along the Z-axis

v_{Xss} the small sinusoidal component of V_X due to coupling between the X-axis equation of motion and the rotational dynamics equation

v_Z the velocity of the rocket along the Z-axis

$v_{\omega y}$ the linear X-axis projection of the y-axis rotational velocity to the center of pressure

x, y, z axes in the rocket frame of reference

X, Y, Z axes in the inertial ground-based frame of reference

α_{at} angle of attack between the total oncoming airstream and the z-axis of the rocket

α_T angle from the Z-axis opposite the direction of the total oncoming airstream

α_y the angle indicating the total rotation about the y-axis axis. In the 2-D model, this is also the angle of the rocket's z axis measured from the Inertial Z axis as the y axis remains aligned with the Y axis

Δ	angle between the direction of travel of the center of gravity of the rocket and the direction the rocket is pointed
Γ	3-D polar coordinate angle of rotation about the Z-axis
ρ	density of air
θ_T	angle from the Z-axis of the angle of the total oncoming airstream
θ_{CG}	angle between the Z-axis and the direction of the movement of the center of gravity of the rocket
Θ	3-D polar coordinate angle from vertical in 3-dimensional space
ϕ, θ, ψ	Euler's angles of rotation
ω_{at}	rotation rate of the angle attack due to the rotational velocity used to calculate the rotational damping moment
ω_n	natural frequency of a second order system
ω_n'	coupled natural frequency of a second order system
ω_y	rate of rotation of the rocket axis frame about the y axis
ζ	damping ratio of a second order system
ζ'	coupled damping ratio of a second order system

10 References

Barrowman, J. (1968). *TIR-33 Calculating the Center of Pressure of a Model Rocket.* Centuri Engineering Company.

Barrowman, J. (1970). *TIR-30 Stability of a Model Rocket In Flight.* Centuri Engineering Company.

Barrowman, J. S. (1967). *The Practical Calculation of the Aerodynamic Characteristics of Slender Finned Vehicles, Master's Thesis.* Washington, D.C.: The Catholic University of America.

Barrowman, J. S., & Barrowman, J. A. (1966). *The Theoretical Prediction of Center of Pressure, NARAM-8.* National Association of Rocketry.

Feretich, B. (2015-2018). *http://www.rafresearch.com/rocketdatalogger/index.html*. Retrieved from RAF Research.

Fetter, T. (2014-2016). *Speedmotion Rockets*. Retrieved from http://speedmotionrockets.com/

Fetter, T. B. (2015, March/April-September/October). Flight Data Analysis using Excel. *Sport Rocketry*.

Fetter, T. B. (2024). *Rotational Dynamic Stability.*

Mandell, G. K. (1968-1969, Oct-Apr). Fundamentals of Dynamic Stability. *Model Rocketry Magazine*.

Mandell, G. K. (n.d.). *Fundamentals of Dynemic Stability, TR-201.* NARTS (National Association of Rocketry).

Mandell, G. K., Caporaso, G. J., & Bengen, W. P. (1973). *Topics in Advanced Model Rocketry.* Cambridge: MIT Press.

Mathcad Home Page. (n.d.). Retrieved from https://www.mathcad.com/en/

McCormick, B. W. (1995). *Aerodynamics Aeronautics and Flight Mechanics.* New York: John Wiley & Sons, Inc.

RockSim. (2024). Retrieved from Apogee Rockets: https://www.apogeerockets.com

Sidi, M. J. (2002). *Spacecraft Dynamics & Control.* Cambridge University Press.

Thomson, W. T. (1986). *Introduction to Space Dynamics.* New York: Dover Publications, Inc.